University of Crete

Department of Materials Science & Technology

“Antibacterial Polymer Coatings on Flexible Substrates”

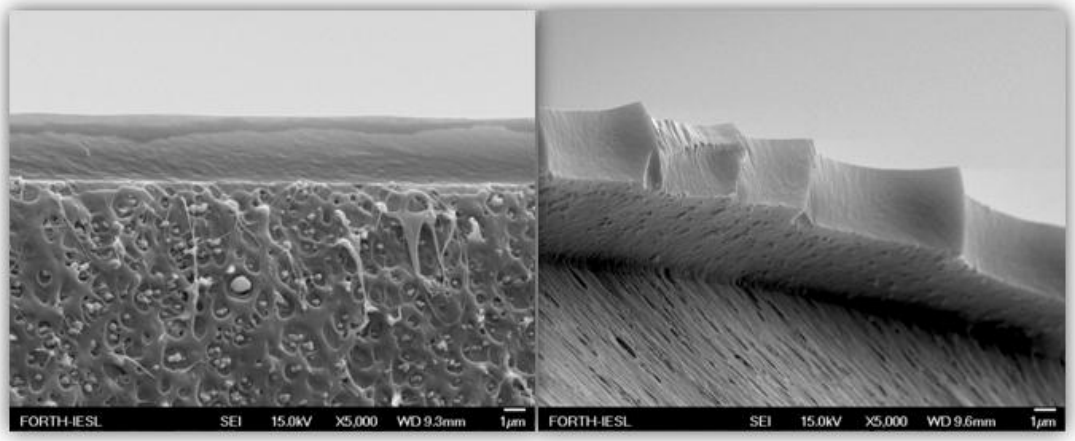

Master Thesis

Nikolaos Konios

Supervisor: Professor Maria Vamvakaki

March 2022

Abstract

Bacterial infections in food comprise a major threat for public health. Ensuring food safety has always been a challenge and therefore, intensive research has been devoted to successfully control microbial growth in food packaging.[1] Recent scientific advances involve the coating of common food packaging materials, including polyethylene and polypropylene films, with non-toxic, antimicrobial polymers.[2, 3] In the present work, water-soluble, natural polymer derivatives were employed to coat flexible food packaging films, and confer them contact-active, antibacterial properties.[4] The coatings, with thicknesses in the micrometer range, were prepared using Mayer rods, whereas their stability and adhesion onto the substrate was achieved using a cross-linker to chemically link the polymer chains among them and also onto the substrate. Fourier transform infrared spectroscopy and field-emission scanning electron microscopy both verified that the coatings were stable and remained intact onto the polyethylene films after one month immersion in water. The coated films presented enhanced antibacterial activity against a range of food-related bacteria, including *Escherichia Coli*, *Listeria Monocytogenes* and *Staphylococcus Aureus*. Notably, the coatings increased the oxygen and water vapor barrier properties of the polyethylene films, without affecting their mechanical strength. The above results suggest that the developed coatings are promising for use in active food packaging technologies.

Acknowledgments

This study started in October 2019 and was completed in December 2021. During this period, I had the opportunity to broaden my research experience and enrich my knowledge in polymer chemistry. I would like to thank Professor Vamvakaki Maria, my supervisor, for giving me this opportunity and for her precious guidance throughout this project under the difficult circumstances of Covid19.

Another important contributor on this study would be Dr. Maria Kaliva for always being there for me, every time I was having trouble solving the problems I came across and for encouraging me every time I needed it. I am also thankful for Dr. Evangelia Vasilaki who was always willing to share with me her experience with coatings. I would also like to thank all the members of the Materials Chemistry lab, Dr. Theodore Manouras, Dr. Eleftherios Koufakis, Maria Psarrou, Maria Karouzou, Dimitris Gounaris, Maya Korthis, Stella Mountaki, Giorgos Karchilakis, Anna Papaioannou, Dimitris Fergadis, Dimitra Gaitanou, Irene Guazzini, Grabriela Gaj, Sylwia Wrobel, Vasilis Tsampalas, Ioanna Hatzaki and Grigoris Karantanais, a former member and a very beloved friend of mine, as well as my dearest friends Iraklis Spiridopoulos, Nikos Dallas, Katerina Stiakaki and Elisavet Karanikola.

I am also really grateful for the excellent collaboration with Ms. Eleni Ouranou, Dr. Dimosthenis Chochlakis and Professor Anna Psaroulaki who also carried out the antimicrobial tests and of course the collaboration with Kolios S.A. and Hatzopoulos S.A. for (among many things) providing us the substrates and carrying out the barrier studies. I could not exclude thanking Professor Maria Chatzinikolaidou who along with Professor Maria Vamvakaki and Professor Anna Psaroulaki have agreed to be in my Masters committee.

Regarding the experiments, I would like to thank Professor Constantinos Stoumpos who was always eager helping me with the oxygen plasma instrument and Aleka Manousaki for her patience with the FE-SEM images, especially with the cross-section imaging that always troubled us.

Finally, from the deepest of my heart I would like to thank my beloved sister Christine, my father Yiannis, my mother Kalliopi for always encouraging me to always go on, never stop and telling me that I can make it.

Thank you very much everyone!!!!!

Table of Contents

Abbreviations

PE: polyethylene

LDPE: Low Density Polyethylene.

LLDPE: Linear Low-Density Polyethylene.

PA: Polyamide

PP: Polypropylene.

CS: Chitosan.

MR: Chitosan modification reagent.

OTR: Oxygen Transmission Rate.

WVTR: Water Vapor Transmission Rate.

FTIR: Fourier Transform Infrared Spectroscopy.

FESEM: Field Emission Scanning Electron Microscopy.

WCA: Static Water Contact Angle.

TGA: Thermogravimetric Analysis.

NMR: Nuclear Magnetic Resonance.

T_m: Melting point.

T_c: Crystallization temperature.

Chapter 1: Introduction

1.1. Food packaging materials

Ensuring food safety has always been a high priority in food industry. The ability to maintain the benefits of their products as well as to retard food deterioration from chemical, biological and physical effects can lead to an improved public health safety and economy. Loss of nutrients, color and taste as well as oxygen and water vapor absorbance, are only a few of the incidents that must be avoided. Therefore, an acceptable food packaging material must create a barrier between the product and its surrounding environment. Furthermore, it has to include adequate mechanical properties that are useful for the rigors of handling, transportation, consumers interaction, abrasion and irradiation. Finally, an appropriate thermal stability is also a requirement for thermal processing such as retort and sterilization processes.[1, 5-8]

1.2. Conventional food packaging materials

The construction and design of appropriate packaging plays a significant role in the shelf life of a food product. An appropriate packaging material affects the product quality and its freshness during storage. Traditional packaging products include glass, metals, paper and plastics. Especially the last one has been introduced in both rigid and flexible forms. It is often considered that the combination of several materials is required for the exploitation of the packaging functional and aesthetic properties.[5-8]

1.2.1. Glass

The use of glass for packaging applications appeared around 3000 BC. The production of glass containers involves the heating of a mixture of silica, sodium carbonate, limestone/calcium carbonate and alumina, to high temperatures. Then, a thick liquid mass is formed that is poured into molders. A few advantages regarding glass include its odorlessness and chemically inert behavior with all food products. Moreover, it is impermeable to gases and vapors, it withstands high processing temperatures and its transparency allows consumers to view the contained product. Even colored glass can be manufactured for the packaging of light-sensitive products. The most important feature of glass is undoubtedly its recyclability. On the other hand, its heavy weight leads to high transportation costs and its rigid properties often leads to breakage from internal pressure or thermal shock.[9]

1.2.2. Metals

Metal also comprises an important and multifunctional packaging form. With aluminum and steel being the most widespread metals used for packaging applications, their features include outstanding barrier properties, formability and recyclability. Derived from bauxite ore, where it exists as alumina, aluminum is used for cans, foil and laminated paper. Its lightweight and excellent barrier properties against moisture, air, odors, microorganisms and chemicals are some of its important features. Aluminum foil is one of the most common forms of aluminum food packaging. They are thin aluminum sheets available in a wide range of thicknesses that allow tight folding. Aluminum is easy to reclaim and process into new products other than aluminum foils. Also, it cannot be welded and has high cost. Tin-free steel which is also known as chrome oxide coated steel is used for the manufacturing of food cans, can ends, trays, bottle caps and closures. Large containers for bulk sale and storage of ingredients can also be achieved. Tin-free steel illustrates adequate formability and strength. Although chrome oxide makes it inappropriate for welding, it is useful for the adhesion of coatings.[5, 10]

1.2.3. Plastics

Plastics are processable materials based on polymers. They are obtained from step-growth and chain-growth polymerizations.

A step-growth polymerization is a step-wise reaction between bi- or multifunctional monomers leading to the formation of high molecular weight polymers after a significant number of steps. Most monomers are consumed early during the reaction forming short chains (oligomers) that can combine to long polymer chains at a later stage. Well-known polymers, natural or synthetic can be obtained from such polymerizations including polyesters, polyethers, polyamides and others.[11]

A chain-growth polymerization involves the growth of a polymer through reactions between unsaturated monomers and active sites. The latter can be either radicals, anions or cations. The mechanism of a chain growth polymerization follows three steps. The first is chain initiation, which involves highly reactive transient molecules (initiators) or active centers to be formed, where energy (i.e., heat, light) is necessary. Subsequently, chain propagation occurs with the addition of monomer molecules to the active chain ends. Lastly, in chain termination all the active chain ends are deactivated by the reaction with other active ends that are present in the system.[12] In chain-growth, polymers are formed by chain addition reactions between monomers without the formation byproducts. Specifically, double or triple bonds of unsaturated monomers break to link and grow polymer chains.

A wide range of advantages can be spotted in plastics. Lightweight and flexible, plastics offer design opportunities as well as molding into various shapes and sheets. Mass transport at low cost is also possible. Thermal stability is another characteristic which is useful as many plastics are heat sealable and their chemical inertness makes it impossible to interact with foods. A main disadvantage of plastics is their poor barrier properties against light, gases, vapors and low molecular weight molecules.[5, 7]

Plastics can be also divided into two major categories regarding their thermal properties: thermosets and thermoplastics. Thermosets are polymers that solidify or set irreversibly when heated, whereas thermoplastics soften upon heating and return to their original state at room temperature. The latter can be easily molded into various products and are therefore good packaging material candidates. All thermoplastics are recyclable but it is worth mentioning that in some cases separation poses practical limitations.[5, 7]

Monomer and component residues such as stabilizers and plasticizers in plastics have triggered health concerns, which led FDA to carefully review all substances used in the manufacturing of plastics. Any substance that could migrate into food is classified as indirect food additive subject to FDA regulations. Despite these safety concerns, the use of plastic keeps rising as a result of their low cost and functional advantages. More than 30 types of plastics have been used as food packaging materials with polyolefins and polyamides being the most common ones.[7]

Polyolefins comprise a group of polymers produced from an olefin or alkene as the monomer. In organic chemistry such monomers are unsaturated chemical molecules containing at least one carbon to carbon double bond. Polyolefins account for approximately 63% of the global polymer production. The two simplest, most inexpensive and predominately used polyolefins are polyethylene and polypropylene. The first one has a simple hydrogen as side group while the latter has a methyl.[7, 13] Their chemical structure is shown in **Figure 1.1**.

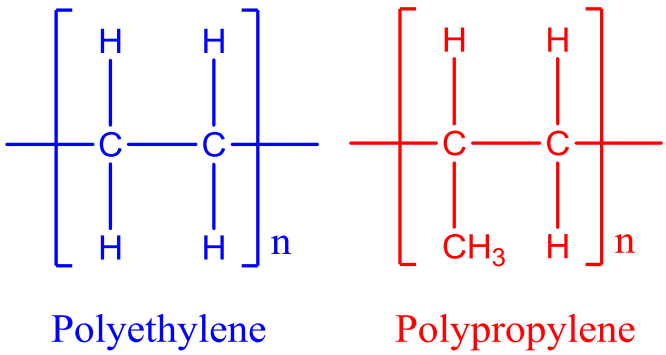

Figure 1.1. Chemical structures of polyethylene and polypropylene.

Regarding polyethylene, there is high-density and low-density polyethylene. The first one is stiff, tough, permeable to gas and easy to process and form and is used for food packaging regularly. Low-density polyethylene is more flexible, and easy to seal, and as it is relatively transparent it poses an appropriate candidate for film applications. On the other hand, polypropylene is harder, denser and more transparent and its significant difference compared to polyethylene is its efficient water vapor barrier properties. In addition, it offers a higher thermal resistance with a melting point at 160 ^{o}C, which is 40 ^{o}C higher than that of polyethylene. A common feature of polyethylene and polypropylene is their chemical inertness. Comprising only carbon and hydrogen atoms and no functional groups that could trigger chemical reactions, it is relatively impossible to interact with foods and ingredients. Therefore, both materials have attracted attention in the food packaging industry.[7, 13, 14]

Polyamides are polymers that occur both naturally and synthetically. The first ones can be proteins such as wool and silk while the latter are produced by step-growth polymerizations of diacid and diamine monomers. Each repeating unit in the polymer is linked with the other one via amide linkages. Similar to olefins, polyamides represent a major class of polymers. They are characterized by a number related to the number of carbon atoms of the originating monomers. For instance, the aliphatic polyamide 6,6 or nylon 6,6, the formation of which is shown in **Figure 1.2**, refers to the six carbon atoms from the hexamethylene diamine monomer and the other six atoms from adipic acid. This kind of polyamide is well known for its high tensile strength and its resistance to abrasion. It can be produced in solid form or as fibers. The latter accounts for more than half of the polyamide manufactured, and are produced for a variety of products like textiles or carpet filaments. Polyamide films have high resistance to heat, stress cracking and puncture. They also have good clarity and are easily thermoformed, while they provide odor and flavor barrier properties. However, it is difficult to heat seal and it is moisture permeable. Fortunately, the latter problems can be overcome by lamination or co-extrusion with polyethylene which creates structures for bacon and cheese packaging.[7, 14, 15]

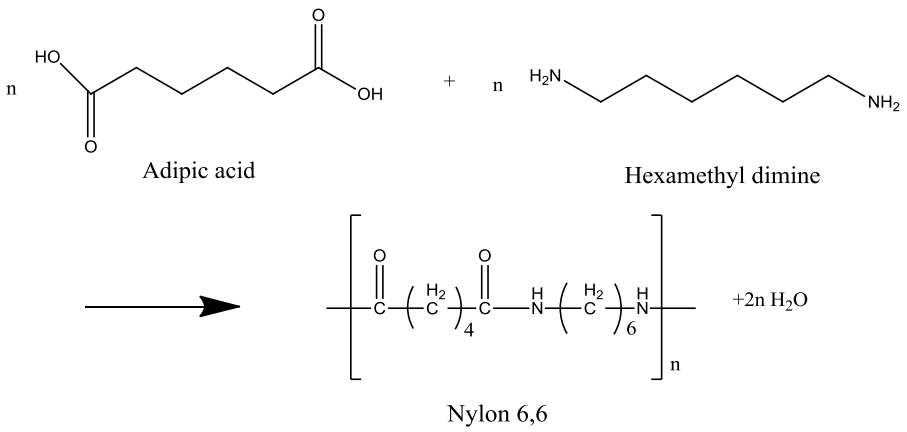

Figure 1.2. Reaction to form Nylon 6,6.

Polyesters is another worth mentioning group of polymers that are widespread used in food packaging industry. They are formed via step-growth polymerizations between difunctionalized monomers containing carboxylic acid and hydroxyl groups. The reaction between terephthalic acid and ethylene glycol results in the formation of the well-known polyester, poly(ethylene terephthalate) (PET), which is shown in **Figure 1.3**. PET has a higher heat resistance compared to olefins and polyamides as it melts above 260 ^{o}C, and it does not shrink below 180 ^{o}C. It is therefore an ideal candidate for heat-sealing and high-temperature applications such as food that can be "boiled in the bag". PET films also illustrate flexibility at -100 ^{o}C and when oriented they show high mechanical strength. However, it offers medium oxygen barrier properties which may be overcome by metallization with aluminum. Finally, when choosing PET as a food packaging material, one must take into account the fact that radicals may be generated that can link with other chemicals and therefore can interact with food and its ingredients.[7, 16]

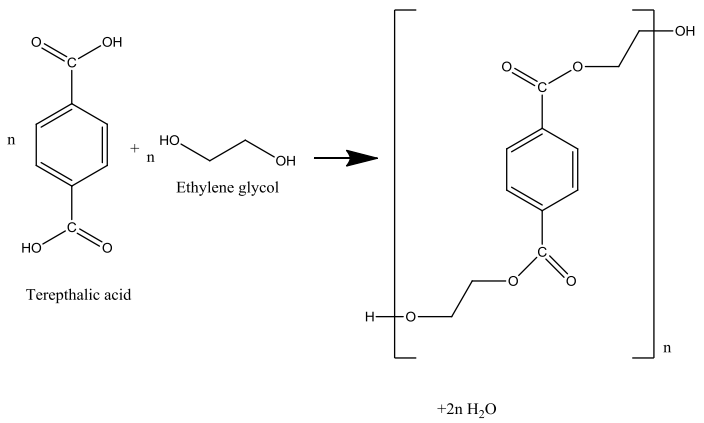

Figure 1.3. Synthetic reaction to prepare poly(ethylene terephthalate).

1.3. Bacterial infections in food packaging

Foodborne infections comprise an issue that challenges food packaging industries. The food production line, from the source to the markets shelves involves unhygienic environments, where the control of the conditions such as temperature and humidity is unattainable leading to bacterial growth and proliferation. These infections are important causes of morbidity and mortality worldwide with an impact on public health and economy, despite the successful controlled programs in developed countries.[5, 6]

Bacteria that are present in food and ingredients vary depending on the type of raw material, production method, handling hygiene and processing. They can cause changes in flavor, odor, color or other sensory properties.[17] Regarding pathogenic bacteria, they can cause illness even if there are no sensory changes. Based on the structure of the cell wall, bacteria can be classified into two groups: gram-positive and gram-negative bacteria.

The cell wall of gram-positive bacteria comprises a complex structure that surrounds the cytoplasmatic membrane. It consists of a peptidoglycan layer that is 40 to 80 layers thick, polysaccharides, teichoic acids and proteins and can absorb substances from the outer environment easily. Gram-positive bacteria may also own a flagella that enhances their movement, and can rarely possess hair-like structures which are known as pili. Two well-known food-borne gram-positive bacteria are *Staphylococcus Aureus* and *Listeria monocytogenes*. The first one has a round shape, varying from 0.5 µm to 1 µm in diameter and it has been passing on for hundreds of years from person to person. *Listeria monocytogenes* has a rod-like morphology, comprising a 0.5-4 µm diameter and 0.5 to 2 µm length. It is important for the food-packaging industries to inhibit this kind of bacteria as it has a 24% mortality rate.[18]

Regarding gram-negative bacteria, they consist of an outer lipid membrane which is not featured as in gram-positive bacteria, making the latter less protected from their outer environment. Gram-negative bacteria have a peptidoglycan layer 2 to 3 nanometers and they can also have flagella or pili. Teichoic acids are not commonly found. A representative gram-negative bacterium that can infect food is *Escherichia Coli*. Similar to *Listeria monocytogenes*, *E. coli* has a rod-like shape with a diameter of approximately 1 µm and a length varying from 1 to 2 µm. Strategies to reduce the number of bacterial cells in food like vegetables and cheese involve pasteurization and domestic cooking. What is interesting about *E. coli* is its heat resistance. In addition, food packaging industries take into consideration the consumers preference for raw or minimally processed food in order to minimize thermal degradation of the nutrients and thus heat processing is not always a preferable method to kill bacteria.[19]

In order to reduce foodborne infections, several strategies have been used to develop antibacterial packaging. These packaging systems, include sachets and pads with volatile antimicrobial compounds or the synergistic action of both volatile and nonvolatile antimicrobial compounds encapsulated directly into the structure of the polymers. Other widespread used methods involve coating or the absorption of antimicrobial compounds onto the surface of a polymeric packaging material, the immobilization of antimicrobial agents onto the polymers and finally the use of polymers that possess inherent antibacterial properties.[20]

1.4. Antimicrobial polymers

Microbial contamination poses a limitation in the shelf life of food and ingredients.[1, 5-7, 21] In addition, other important epidemiological situations, including nosocomial infections and infections by surgical and dental equipment, have attracted the attention of biochemical and physicochemical research to focus on macromolecules and polymers with antibacterial properties.[22] An antibacterial substance can be considered as an agent that kills microbes or inhibits their proliferation. Antimicrobial polymers were first studied in 1965, featuring remarkable efficiencies compared to their small molecular counterparts. Since then, intensive development of macromolecular science has led to the synthesis of novel polymers and the modification of known polymers to bear antimicrobial properties.[22]

When microbes adhere to surfaces, they excrete components to create biofilm in order to bind. Biofilm is a polymeric conglomeration composed of components, such as polysaccharides, proteins and DNA. Defective biofilms cannot enhance microbes' proliferation and therefore antibacterial polymers focus on preventing the adhesion of microbes and their viability.[22] According to the mechanism of antibacterial activity, antimicrobial polymers can be categorized as passive or active.[22, 23]

Passive action focuses on preventing the adsorption of proteins on the surfaces making the microbes unable to adhere, without killing them. The ability of a surface to repel or resist the initial attachment of bacteria is known as antifouling effect. Well-known passive polymers comprise self-healing, slippery liquid-infused porous surface such as polydimethylsiloxane, uncharged polymers like poly(ethylene glycol) (PEG) and charged ampholytes and zwitterionic polymers such as phosphobetaine. The most important and widespread studied polymer among the previous is PEG. PEG reduces dramatically protein adsorption and it is the most commonly used as passive antibacterial material due to its high chain mobility, large exclusion volume and steric hindrance effect. What is worth mentioning about the antifouling effect is that it can be widely found in nature. Indeed, insect wings, shark skin and lotus wings

show such properties by preventing contaminating particles, algae spores and bacterial cells to adhere.[22, 23]

Active action involves polymers that actively kill bacteria that adhere to surfaces when in contact, an effect known as bactericidal. Such polymers comprise active agents like cations. The mechanism of action is not yet completely understood, however one of the prevailed theories claims either the penetration of the polymer in the cell wall destroying the cytoplasmatic membrane and creating leakages that lead to cell death or the attraction of useful components from the cell that leads to leakages and cell death. The most widely used active antimicrobial polymers are functionalized with positively charged quaternary ammonium groups. Other polymers, like polyethyleneimine interacts through electrostatic interactions with the cell membrane leading to its rupture. Polyguanidine adheres and subsequently disrupts the Ca^{2+} salt bridges.[22, 23]

Antimicrobial polymers may also be sub-categorized as leaching and non-leaching polymers. The first type releases an antimicrobial agent which will trigger the antimicrobial effect after its chemical interaction with gems. Non-leaching antimicrobial polymers have immobilized antimicrobial agents which generate a positively charged surface, that mediates the antimicrobial activity by a physical effect. For this, the germs need direct contact with the material surface. **Figure 1.4** illustrates the differences of the leaching and non-leaching antimicrobial polymers.[24]

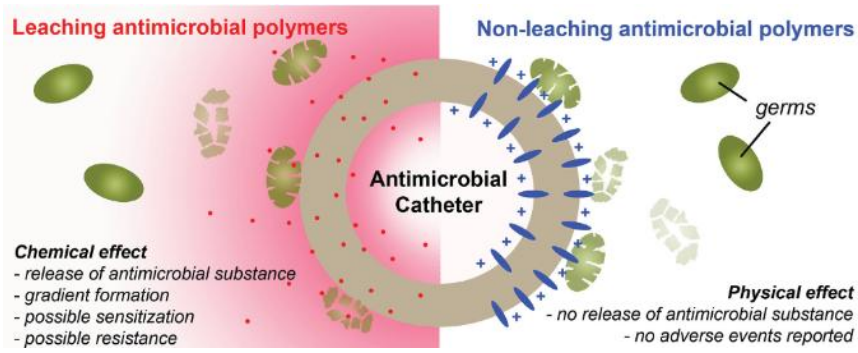

Figure 1.4. Schematic representation of the different mode of action of leaching and non-leaching antimicrobial polymers.[24]

Abundant surfaces can be found in nature and have been widely investigated for their possible antimicrobial effects. They comprise an inexhaustible source of inspiration for researchers to develop materials with similar modes of action. For instance, insects like cicada were found to have wings that are bactericidal. This effect is not chemical, but is attributed to the surface nanostructure of the wing. Despite the fact that cells can attach to the wings, they are consequently

mechanically ruptured by the action of the surface nanopattern within a short time after the attachment. Such interactions can inspire researchers to develop surfaces with similar nanostructures. **Figure 1.5** shows a schematic representation of the cell attachment and the consequent rupture.[24, 25]

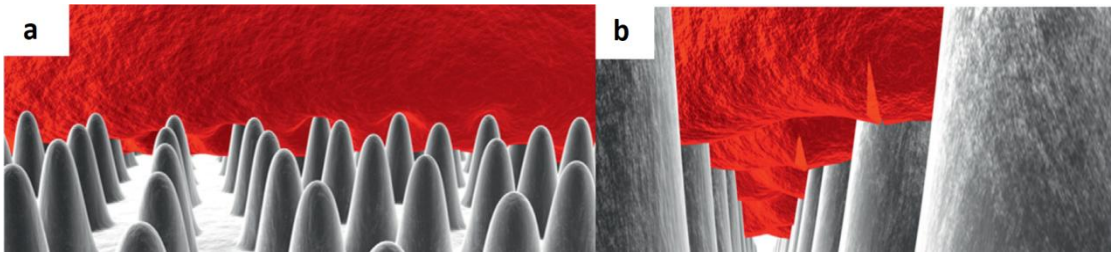

Figure 1.5. Schematic representation of cell attachment on the cicada nanopillars (a) and rupture from the special wing nano-pattern.[23, 25]

1.5. Antimicrobial properties of chitosan

Polymers acting as antibacterial agents find a vast range of applications. The World Health Organization has been expressing its worries regarding the severe side effects of antibiotics, such as neurotoxicity and antibiotic resistance.[22] Medical devices and food consumption comprise important infection pathways and the demand for avoiding such events, has led scientists to develop polymer-based materials with enhanced antibacterial properties. Since the fields of application of such materials require substantial amounts of material as well as lack of toxicity and biodegradability, researchers have focused on studying natural polymers which are abundant.[22]

Chitosan, is among the most widespread and studied non-toxic and biodegradable natural polymers. It is a linear polysaccharide comprising two types of randomly distributed repeat units, namely β-(1-4)-linked D-glucosamine, which is also known as the deacetylated unit and N-acetyl-D-glucosamine or acetylated unit. Chitosan is derived from the partial deacetylation of chitin which is found in the exoskeleton of crustaceans and the cell walls of fungi. The deacetylation reaction of chitin involves a simple treatment of the polymer in alkaline environment. The degree of deacetylation may vary and can be easily calculated by ^{1}HNMR spectroscopy.[3, 26]

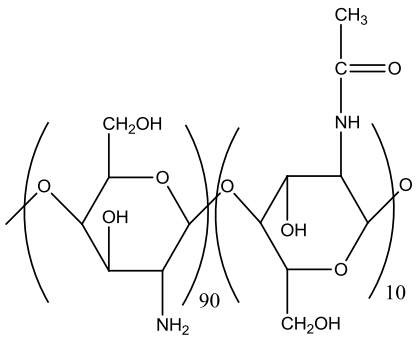

Figure 1.6. Chemical structure of chitosan with 90% degree of deacetylation.

Figure 1.6 shows the chemical structure of chitosan. Chitosan is a weak base due to the presence of the primary amine group in its structure. Chitosan is water-soluble at low pH values upon the protonation of the amine groups.[27] It also contains primary and a secondary hydroxyl group that can be used for a variety of reactions. Regarding its antibacterial activity, chitosan can inherently kill bacteria once its amine groups are protonated.[27, 28] In acidic environment, the positively charged units interact with the negatively charged moieties of the bacterial components. Both water solubility and the antibacterial properties of chitosan are influenced by the solution pH. The degree of deacetylation determines the primary amine group content and therefore, its antibacterial properties. Finally, it is proposed that low molecular weight chitosan is more effective against bacteria compared to higher molecular weight polymers, because the positively charged groups penetrate the cell envelope easier.[22, 27]

1.6. Chitosan coatings on conventional packaging materials

Regarding the applications of chitosan in the food industry, it has been used as a coating in meat products,[29] eggs[30] and fruit.[31] It has been reported that chitosan can effectively kill gram-negative and gram-positive bacteria and fungi and can also enhance the barrier properties of the packaging materials preventing ripening, water loss and oxygen permeation.[26, 32] However, chitosan coatings on conventional packaging materials such as polyethylene and polypropylene are challenging due to the poor wettability of the latter by water. In addition, both polyethylene and polypropylene have no functional groups but rather comprise long aliphatic chains of hydrogen and carbon.[33]

In order to overcome to poor water wettability of common packaging materials such as polyethylene and polypropylene, industries use plasma technology to modify the surface of the flexible substrates from hydrophobic to hydrophilic and improve their adhesion properties without changing their bulk properties. The speed of this method is high and only a few minutes of application are required, which is beneficial as it reduces energy consumption and allows continuous in-line

processing. Oxygen is usually employed as a gas, which is used to generate radicals that can initiate physicochemical modifications within the depth of a few nanometers on the surface of polymer films.[34]

However, polyethylene and polypropylene are polymers comprising both crystalline and amorphous regions. In the latter regions, mobility of the chains occurs in response to interfacial forces and the polymers adapt their surface chemical structure to the environment. This leads to the recovery of the hydrophobicity, which is depended on the crystallinity of the polymeric material as well as other parameters of the plasma process, such as time and intensity. For instance, in highly crystalline polymers, hydrophobic recovery may be reduced because of the highly restricted mobility in the crystalline regions. Consequently, limited rotational and translational motions in the surface region can reduce the aging rate of polar groups that are present after plasma treatment.[34]

1.7. Aim of the present work

In the present work, water-soluble natural polymer derivatives were employed to coat flexible food packaging films and confer them contact-active, antibacterial properties. Food packaging films comprising a polyethylene top layer and polyamide bottom layer were first treated with oxygen plasma to improve the water wettability and adhesion properties of the polyethylene surface. Consequently, coatings in the micrometer range were prepared using Mayer rods, whereas their stability and adhesion onto the substrate was achieved using a cross-linker to chemically link the polymer chains among them and onto the substrate. Fourier transform infrared spectroscopy and field-emission scanning electron microscopy were used to verify the stability of the coatings onto the polyethylene surface after one month immersion in water. Furthermore, gram-positive bacteria, namely *Staphylococcus Aureus* and *Listeria Monocytogenes*, and the gram-negative *Escherichia Coli*, were used to determine the antibacterial properties of the coatings. Finally, the influence of the coatings on the mechanical, thermal and barrier properties of the packaging films was investigated proving that the developed coated substrates are promising for use in active food packaging technologies.

Chapter 2: Experimental part

2.1. Materials and chemical reagents

Multilayer substrates comprising a linear low-density polyethylene, (PE, inner surface) and polyamide (PA, outer surface) with a 110 ± 10 μm thickness were provided by Kolios S.A. Chitosan (CS, 30000 g/mole, 10 cps) was purchased from Glentham Life Sciences and acetic acid (glacial) from Scharlau. The Modification Reagent (MR, ≥ 90% purity) was purchased from Sigma-Aldrich. Ethanol (EtOH, ≥ 98% purity, denaturated with MEK, IPA and Bitrex) and Acetone (≥ 99.8% purity) were purchased from Honeywell. Acetic acid (≥ 99% purity) was purchased from Sigma Aldrich. Mili-Q water was obtained from a milipore apparatus with a resistivity of 18.2 MΩ at 298 K and was used for all experiments.

2.2. Chemical modification of chitosan

In a 500 mL flask, a 3 cm length magnetic stirrer bar, 5 g of chitosan, 297 mL Mili-Q water and 3 mL of acetic acid were added. The temperature was set to 80 ^{o}C and the stirring rate at 600 rpm. After 1 h stirring, a yellowish transparent solution was obtained. Then, MR was added (at a final molar ratio of MR/Chitosan = 6) in four doses every 20 min. The reaction was left overnight under stirring. The next day, the reaction medium was precipitated dropwise in acetone, the volume of which was four times the volume of the reaction. After filtration, the product was left in ethanol overnight at 40 ^{o}C to remove any unreacted MR. After verifying the successful purification of the polymer from MR residues by ^{1}H NMR spectroscopy, the product was diluted in water and was freeze dried at -40 ^{o}C overnight.

2.3. Oxygen plasma treatment of the polyethylene surface

The surface of polyethylene exhibits poor water wettability and it is therefore difficult to coat with water soluble polymers such as modified chitosan. In order to improve its water wettability, oxygen plasma is used to introduce carboxyl groups on the surface. A 10x20 cm^2 polyethylene film was set on glass and placed in the plasma chamber. After allowing the instrument to evacuate for about 5 min, the oxygen valve was turned on. Parameters of the plasma treatment were then optimized. Briefly, oxygen pressure was set to 0.5 mbar, the intensity at 89 Watt and finally the timer at 3.5 min. At the end, the vacuum and oxygen were turned off and the chamber was set to ventilation.

2.4. Coating of chitosan and modified chitosan on the plasma pre-treated polyethene surface

After the successful oxygen plasma treatment of the polyethylene surface, coatings of chitosan and modified chitosan were developed. For the fabrication of chitosan coatings, a 0.05 g/ml aqueous solution of chitosan was prepared. The pH of the solution was optimized at 3.6 with the addition of acetic acid (8 v/v % in water). Crosslinker was further added at a 0.35 crosslinker/chitosan molar ratio. Subsequently, 1 ml of the solution was placed in a syringe and was deposited on the edge of a 10x20 cm^2 polyethylene surface. A metering rod was used to spread the solution on the surface which led to a homogenous coating. The coating process is represented schematically in **Figure 2.1**.

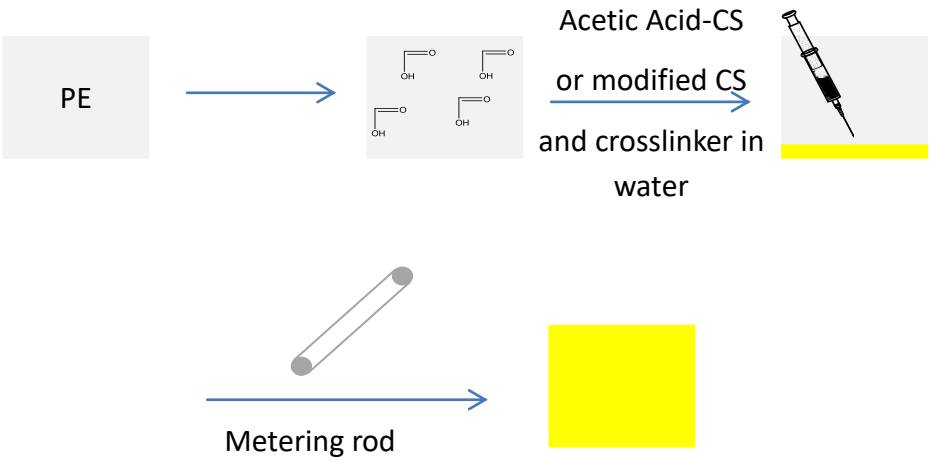

Figure 2.1. Schematic representation of the coating process.

A similar procedure was also followed for the preparation of coatings based on modified chitosan. Contrary to chitosan, the pH value of the aqueous solution of modified chitosan was optimized at 5.2 with the addition of acetic acid (0.25 v/v % in water).

2.5. Characterization techniques

2.5.1. Scanning Electron Microscopy (SEM)

An electron microscope operates using the same basic principles as the optical microscope, but uses electrons instead of light. Because the wavelength of electrons is much smaller than that of visible light, the optimal resolution attainable by an electron microscope is many orders of magnitude higher than that of an optical microscope. Thus, electron microscopes can reveal the finest details of internal

structure – in some cases as small as individual atoms. Scanning and transmission electron microscopes are two widely used microscopes in research, for which the imaging is derived from the electron-specimen interactions.[35]

A scanning electron microscope uses a focused beam of high-energy electrons and generates 3 types of signals, backscattered electrons, X-rays and secondary electrons, at the surface of the specimens. Information regarding the external morphology, chemical composition and crystalline structure can be obtained by rastering the beam across the surface in a series of parallel lines. The sample is mounted on a stage that can be accurately moved in the x, y and z directions. A schematic representation of a SEM setup is illustrated in **Figure 2.2**.

In order to produce the high energy beam of electrons needed for imaging, the instrument operates under high vacuum and in a dry environment. The electrical conductivity of the specimen has to be high enough to ensure that the majority of the incoming electrons go to the ground and do not charge the sample. For this purpose, the samples are coated with conductive materials, such as gold or platinum.

The primary electron beam interacts with the sample over the interaction volume and generates three signals. Backscattered electrons are beam electrons that undergo multiple scattering in the interaction volume and are reflected from the sample. Elemental contrast of the sample is derived from this type of electrons, because heavier atoms scatter more electrons. Secondary electrons, emitted from very close to the specimen surface, can produce very high-resolution images of a sample surface, revealing details less than 1 nm in size. Finally, the energy or wavelength of the characteristic X-rays can be measured by energy-dispersive X-ray spectroscopy or wavelength-dispersive X-ray spectroscopy and are used to identify and measure the abundance of elements in the sample and map their distribution.

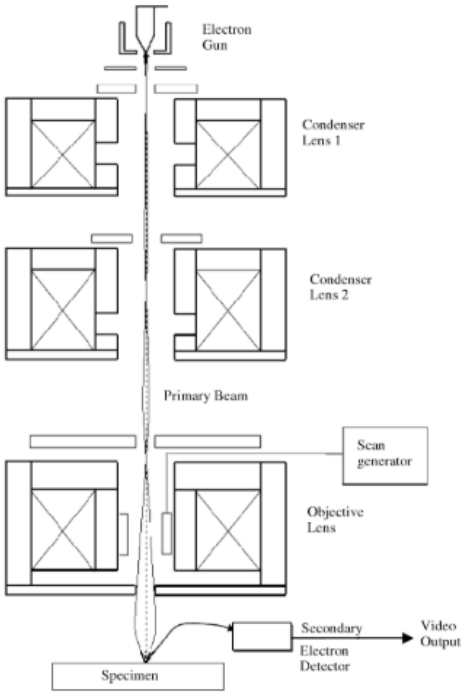

Figure 2.2. Schematic representation of a scanning electron microscope setup [35].

SEM images were recorded on a JEOL JSM-6390LV instrument at an electron acceleration voltage of 15 kV. Polyethylene films 1x1 cm^2 were placed on carbon tape. Then, the samples were sputter-coated with Au (10 nm thickness) before imaging.

2.5.2. Thermogravimetric analysis (TGA)

Thermogravimetric analysis (TGA) is a technique which measures mass differences between a sample and a reference as a function of the applied temperature or as a function of time. The instrument involves a thermocouple that is used to record the temperature automatically, a precision balance to measure the weight of the sample and of a reference, while a computer controls the temperature and collects data.[36]

The measurement can be performed under different atmospheres, oxidative or inert (nitrogen, argon, helium). The output of a TGA measurement are curves that show changes in mass or curves that display enthalpy changes. These changes may be caused by evaporation of volatile substances, oxidation (when oxidizing atmosphere is applied), thermal decomposition of matter, changes in magnetic properties and heterogeneous chemical reactions.

It is possible to identify every phenomenon carried out during the measurement. For instance, under an inert gas atmosphere and constant heating rate, volatile matter is expected to evaporate up to 200 °C, whereas organic matter undergoes pyrolysis up

to 600 °C. Inorganic matter that may be contained in the material (e.g., clays, salts) are not altered and are left as residues.

A Perkin Elmer thermal analyzer, model Diamond TG/DTA, was used in the present study. The results were collected using the Diamond Pyris software. 10 mg of dried sample were heated under a nitrogen atmosphere, at a heating rate of 10 °C/min up to 600 °C.

2.5.3. Fourier transform infrared (FTIR) spectroscopy.

Fourier transform infrared (FTIR) spectroscopy is a widely applicable spectroscopic technique used to obtain information about the chemical functional groups of a substance.

FTIR spectroscopy is based on the interaction of electromagnetic radiation with the electrical dipole of a molecule. When molecules are irradiated with infrared light, excitation of their vibration bonds occur.[37] Vibrations fall into the basic categories of stretching and bending. A stretching vibration involves a continuous change in the interatomic distance along the axis of the bond between two atoms, while bending vibrations are characterized by a change in the angle between two bonds. The various types of vibrations are shown schematically in **Figure 2.3**.

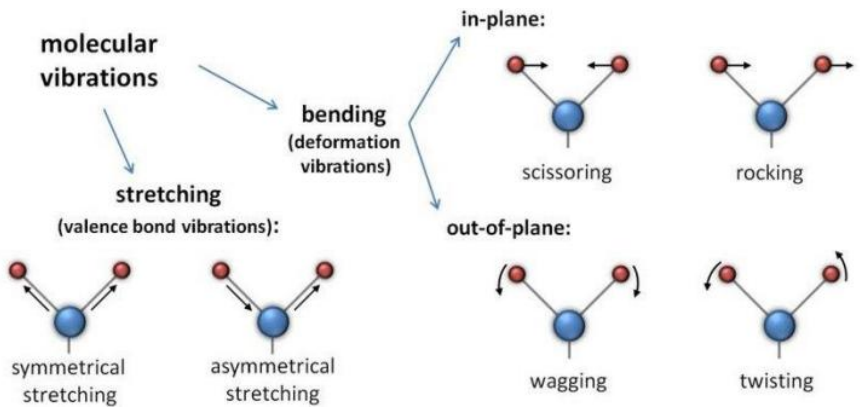

Figure 2.3: Types of molecular vibrations.[37]

Specific interatomic bonds absorb infrared light at particular wavenumbers, regardless of the response of the other chemical bonds in the rest of the molecule, which can be used to identify the structure of molecules.

Samples for FTIR spectroscopy were dried and about 10 mg of the sample were analyzed using the optical spectrometer Nicolet 6700. 2x2 cm^2 polyethylene film samples were used.

2.5.4. Nuclear magnetic resonance (NMR) spectroscopy

Nuclear Magnetic Resonance is an analytical method that is widespread used for the identification of the chemical structure of organic substances. It is based on the principle of positively charged nuclei that are spinning on an axis leading to a weak magnetic field.[38]

When no external field B_o is present, the magnetic field of the nuclei is randomly oriented, whereas in the presence of an external field the magnetic field of the nuclei either align or oppose to it. It is worth noting that when the two fields align, the energy required is lower and therefore this state is preferred over the opposing one. Once the oriented nuclei are irradiated with electromagnetic irradiation of appropriate frequency, energy absorption takes place and the state with the lower energy reverts to the state with the highest energy, which means that the nuclei are resonated with the applied irradiation.

Regarding the frequency needed for resonance, it depends on the strength of the external magnetic field and on the type of the nucleus. The stronger the magnetic field, the higher is the energy difference between the two spin states. This means that the radiation required is of higher frequency for spin reversal to take place. If the magnetic field used is weaker, the energy required for the reversal of the spin to take place is lower.

Every nucleus with an odd number of protons, ^{1}H, ^{14}N, ^{31}P to name a few, and all the nuclei with an odd number of neutrons, such as ^{13}C, can trigger magnetic resonance. However, nuclei with an even number of protons and neutrons, like ^{16}O, cannot exhibit this phenomenon.

It should be noted that the absorption frequency is not the same for all the nuclei in a molecule. Electrons form their own microscopic local magnetic fields upon the application of an external field. Such fields act contrary to the external filed, leading to a lower field in the nucleus compared to the external. It can be concluded that nuclei are protected from the external field due to the surrounding electrons. While each nucleus in a molecule has a specific electronic environment, the real magnetic field is not the same for each nucleus. NMR can map the elements of an organic compound by the different times at which a nucleus resonates with the magnetic field.

NMR signals are gathered in graphs that show the increase of the magnetic field from left to right. The left part of the graph is the downfield region and the right part of the graph is the upfield region. To determine the absorption site, the NMR graph is graded and a reference point is used. The nuclei that are highly protected by the electrons need stronger exercised field in order to resonate and they absorb on the right side of the graph. The nuclei that are less protected need weaker exercised field to resonate, and they absorb on the left side of the spectrum.

Finally, what is often noticed in an NMR spectrum is the splitting of the absorption of a proton into multiple peaks. The phenomenon of multiple peaks is caused by the interaction or coupling of the nuclear spin of nearby atoms. Specifically, the microscopic magnetic field of a nucleus affects the magnetic field that the nearby nuclei recognize. The differences in the extent of the electronic protection are due to the differences in the chemical shift among nuclei. In general, protons with ν equivalent nearby protons, show ν+1 peaks in the NMR spectrum.

Samples for NMR analysis were prepared by dissolving about 10 mg of a sample in 200 μL deuterium oxide and were then placed in NMR tubes.

2.5.5. Mechanical properties of the PE-based substrates

The mechanical properties of the materials reveal their behavior under an applied force. A tensile test involves the loading of a specimen in a controlled manner as well as the measurement of the applied load and the elongation of the specimen over a distance.[39] The identification of various tensile properties such as the young modulus, elasticity, elastic limit, yield point and yield strength can be determined by such tests.

The most common curve obtained from tensile tests is the stress versus strain plot. The stress is the load P, applied to the original cross-sectional area of the specimen A, and is defined as $\frac{P}{A_o}$. Strain ε is expressed as $\varepsilon = \frac{L-L_o}{L_o}$, where L_o is the initial length of the specimen and L is the final length. A main requirement for the calculation of the both stress and the strain is the geometry information of the specimen, namely the thickness, length and width. A typical stress-strain plot is shown below.

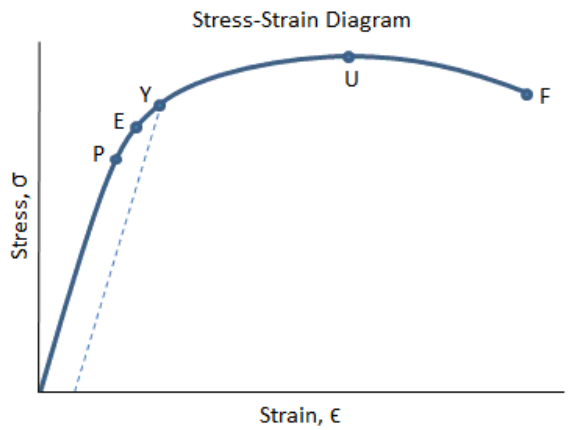

Figure 2.4. Typical stress-strain curve.[39]

As shown in **Figure 2.4**, both the stress and the strain increase in a linear manner initially until the limit **P** is reached. This is the elastic part of the curve revealing that

when the force is released the specimen will return to its initial shape. In this region, Hooke's law, which is expressed as $\sigma = E*\varepsilon$, can be applied and the Young modulus E can be calculated.

Secondly, **E** in **Figure 2.4** stands for the elastic limit, which represents the maximum value of stress at which there is no permanent set. Even though the curve is not linear between the proportionality limit and the elastic limit, the material is still elastic in this region and if the load is removed, at or below this point, the specimen will return to its original length.

Furthermore, the **Y** point in the curve is the yield point, which represents the value of stress above which the strain will begin to increase rapidly. The stress at the yield point is called the yield strength, S_{ty}. For materials without a well-defined yield point, it is typically defined using the 0.2% offset method in which a line parallel to the linear portion of the curve is drawn that intersects the x-axis at a strain value of 0.002. The point at which the line intersects the stress-strain curve is designated as the yield point.

U is the point corresponding to the tensile strength, S_{tu}, which is the maximum value of stress on the stress-strain diagram. After reaching the ultimate stress, specimens of ductile materials will exhibit necking, in which the cross-sectional area in a localized region of the specimen reduces significantly.

Finally, **F** is the fracture point or the break point, which is the point at which the material fails and separates into two pieces.

Regarding the tensile studies on the PA-PE film carried out in this work, samples were cut in 10x1.5 cm^2 pieces. The test speed was optimized at 100 mm/min and samples were exerted at an initial force of 2 Newtons. Each test was repeated in both the transversal and the machine direction of the film.

2.5.6. Barrier studies: oxygen and water vapor transmission rate measurements

Oxygen is a critical mass transfer component in several deteriorative reactions that can influence the shelf-life of a plastic film. Oxygen-barrier properties are typically measured by means of oxygen permeation (OTR) which is expressed in cm^3/m^2*day*atm. The permeability unit is the oxygen gas volume permeated through the coated film per effective area of one m^2 and thickness of one mm in 24 h under a pressure difference of 1 atm.[40]

Water Vapor Transmission Rate (WVTR) is the steady state rate at which water vapor permeates through a film at specified conditions of temperature and relative humidity. Values are expressed in $g/m^2/24$ h in SI units.[41]

Barrier studies were carried out by Hatzopoulos S.A. 20x10 cm^2 samples were studied for their oxygen transmission rate (23 ^oC) and water vapor transmission rate (38 ^oC).

2.5.7. Static water contact angle measurements

Water contact angle (WCA) measurements are used for the estimation of the wettability of a solid surface. The contact angle, θ, is defined geometrically as the angle formed by a liquid at the three-phase boundary where a liquid, gas and solid intersect. At a given temperature and pressure, a given system of solid, liquid, and vapor has a unique equilibrium contact angle. The sessile drop or static contact angle is the simplest contact angle technique. This is when the liquid drop is static on the surface. However, depending on the characteristics such as the chemical homogeneity, topography and roughness, there are a variety of contact angles measured on surfaces.[42]

Dynamic advancing and receding contact angles can be measured to capture the whole range of angles for a particular surface. The discrepancy between the advancing and retreating angles is defined as contact angle hysteresis. Hysteresis is caused by the chemical and topographical heterogeneity of a surface, solution impurities absorbing on the surface, swelling, rearrangement, or change of the surface by the solvent. Modern optical tensiometers analyze the liquid's drop shape by taking images of the drop with a digital camera. The drop is then fit with the Young-Laplace equation with the tangent line drawn from the baseline of the drop to the edge. The droplet can be dispensed either manually, or automatically, but in both cases, a given volume of water is deposited on the surface of interest by a needle tip or pipette that is gently brought into contact with the surface of interest.

The wettability of the coated polymer films prepared in this work was assessed by static WCA measurements using a contact angle goniometer (OCA- 40, DataPhysics Instruments GmbH, Filderstadt, Germany) and the sessile drop method. A 4 µL droplet of nanopure water was used and the contact angles were calculated from the digital images of the water droplets deposited on the surfaces, recorded by a camera, using the appropriate software. Each measurement was carried out three times.

2.5.8. Differential scanning calorimetry (DSC)

Differential scanning calorimetry (DSC) is a technique used for the thermal analysis of various materials including polymers. DSC tracks the heat capacity (Cp) of a sample by measuring the changes in the heat flow during consecutive heating and cooling cycles. This allows the detection of several physical phenomena like phase transitions, melting points, crystallization and glass transition. The most common type of DSC is the heat-flux, in which a sample of a known mass, enclosed in a pan, and an empty reference pan are placed on a thermoelectric disk surrounded by a furnace. When the furnace is heated, both pans are heated through the thermoelectric holder and the heat flow is calculated by the difference in temperature (ΔT) between the sample and the reference. This difference would be the amount of excess heat absorbed or released by the sample during an endothermic or exothermic process, respectively. Endothermic and exothermic processes like melting and crystallization respectively, are shown as peaks. Regarding the glass transition of amorphous or semicrystalline materials, it is shown as a step on the baseline of the curve.[43]

A Perkin-Elmer Diamond DSC was used for the present study. Samples of 8 to 12 mg were used and the analysis took place from 0 to 200 ^{o}C at a 10 ^{o}C/min rate for the heating and cooling cycles, respectively.

2.5.9. Oxygen plasma treatment of the PE substrates

Plasma can be described as a partially ionized gas comprising neutral atoms, atomic ions, electrons, molecular ions, and molecules present in excited and ground states. The charges balance each other and therefore a significant number of these charges are electrically neutral. The charged particles present in plasma are responsible for its high electrical conductivity. Since plasma consists of electrons, molecules or neutral gas atoms, positive ions, UV light along with excited gas molecules and atoms, it carries a large amount of internal energy. All molecules, ions and atoms interact with a particular surface leading to either cleaning, activation, deposition and etching of the surface. Hence, by selecting a gas mixture, pressure and power the effects of plasma treatment on any surface can be specified or precisely tuned.[34]
Plasma treatment is usually performed within a chamber or enclosure that's evacuated (vacuum plasma). The air within the chamber or enclosure is pumped out prior to letting gas in. The gas then flows in the enclosure at a low pressure. This is done before any energy (electrical power) is applied.
On industrial scale, oxygen is used as a gas for processing a variety of substrates. Applying plasma treatment on plastic surfaces like polyethylene and polypropylene can result in an effective surface activation before any gluing, printing or lacquering

could take place. The process leads to the deposition of functional groups like carbonyl and hydroxyl groups on the substrate, improving the adhesion properties and hydrophilicity. Similarly, materials like ceramics and glass can also be treated with plasma.

A plasma cleaner Zepto model 2 from Diener electronic was used in all experiments. In this work, a 10x20 cm^2 polyethylene films were immobilized on glass and placed in the plasma chamber. Oxygen pressure was set to 0.5 mbar, the intensity at 89 Watt and finally the timer at 3.5 min. The coating of the films took place within one hour after plasma treatment.

2.5.10. Antimicrobial tests

Antimicrobial tests were carried out by Miss Eleni Ouranou and Dr. Dimosthenis Chochlakis in Prof. Psaroulaki's group. Regarding the identification and quantification of the antimicrobial action of the commercial and coated PE, the method used is in agreement with the ISO22196/2011 protocol. In all experiments, strains of *Staphylococcus Aureus* (*S. aureus*, ATTC658P), *Escherichia Coli* (*E. coli*, ATTC8739) and *Listeria Monocytogenes* (*L. monocytogenes*) (Food, Water and Environment Sector, Medical School of the University of Crete) were used.[44]

A colony-forming unit is transferred to nutrient agar with a sterilized metallic rod. Subsequently, incubation at 35 ± 1 ^{o}C for 16-24 hours takes place (Bacterial growth A). Bacteria from the latter are placed to a fresh slant growth, where they are incubated at 35 ± 1 ^{o}C for 16-20 h (Bacterial growth B). It is estimated that the bacteria population is at the bacteriostatic growth phase.

In order to prepare the inoculum, a colony forming unit is transferred with a sterilized metallic rod from bacterial growth B to a nutrient broth (NB) at a 1/500 ratio. With a photometer at OD = 600 nm and by optimizing the NB volume the bacterial concentration is set from $2.5*10^5$ to $10*10^5$ cell/ml targeting $6*10^5$ cells/ml.

In each test, 9 samples are used to repeat the experiment 3 times. 6 samples are used as control (commercial PE) and 3 for the estimation of the antimicrobial action (CS or modified CS coated PE). Regarding the control samples, 3 of them are used for measurements after the cell inoculation and the other 3 are measured after 24 h. In addition, the 3 coated samples are measured 24 h after inoculation.

Consequently, 10 ml of Soya Casein Digest Lecithin Polysorbate *Broth* (*SCDLP*) was added to the samples in order to recover the bacteria. Then the SCDLP broth is diluted with phosphate buffered physiological saline. 1 ml of the undiluted broth and 1 ml of diluted broth were added in two Petri dishes. 15 ml plate count agar (PCA) is added to each dish and incubation takes place at 35 ± 1 ^{o}C for 40-48 h. The colonies

in each dish are measured and the microbial load, N, of the substrate is evaluated according to the following formula:

$$N = \frac{100 * C * D * V}{A} \quad (1)$$

Where, N is the number of living cells per substrate cm^2, C is the average colonial number in the two petri dishes, D is the dilution where the colonies where measured, V is the volume of SCDLP that was added to the petri dish for the bacterial recovery and A is the surface of the substrate in mm^2.

An accurate log value of the number of living cells that were recovered after inoculation must valid the following equality:

$$(L_{max} - L_{min})/L_{mean} \leq 0.2$$

Where, L_{max} is the log10 of the maximum number of living cells, L_{min} the log10 of the minimum number of living cells and L_{mean} is the the log10 of the average number of cells that were recovered from the substrate. The average number of recovered living cells in the control substrates after inoculation must be between $6.2*10^3$ cells/ cm^2 and $2.5*10^4$ cells/cm^2.

Finally, the antimicrobial action of the substrate is evaluated according to the following formula:

$$R= (U_t - U_o) - (A_t - U_o) = U_t - A_t$$

Where, R is the antimicrobial action rate, U_o is the log10 of the number of living cells per cm^2 recovered immediately after inoculation, U_t is the log10 of the number of living cells per cm^2 that were recovered after 24 h incubation and A_t is the average log10 of the number of living cells per cm^2 recovered from the coated substrates after 24 h incubation.

Chapter 3: Results and Discussion

3.1. Characterization of chitosan

Chitosan 30000 g/mol, 10 cps, 90 wt% deacetylation (data from Glentham Life Sciences) was chosen to coat the multilayer packaging materials based on polyethylene and polyamide. Before the development of the coatings the physicochemical properties of the biopolymer were characterized.

3.1.1. Characterization of chitosan and modified chitosan by ^{1}H NMR spectroscopy

Figure 3.1 shows the ^{1}H NMR spectrum of chitosan used in all experiments. The peak **1** at 0.05 ppm is attributed to the three methyl protons of the acetyl group. The peak **2** at 1.2 ppm represents the proton of the carbon that is linked to the primary amine group. Next, the peaks present between 1.4 and 2 ppm are attributed to the protons **3, 4, 5, 6** and **7** of chitosan. Finally, the peak at 2.9 ppm is attributed to proton **8**.[45]

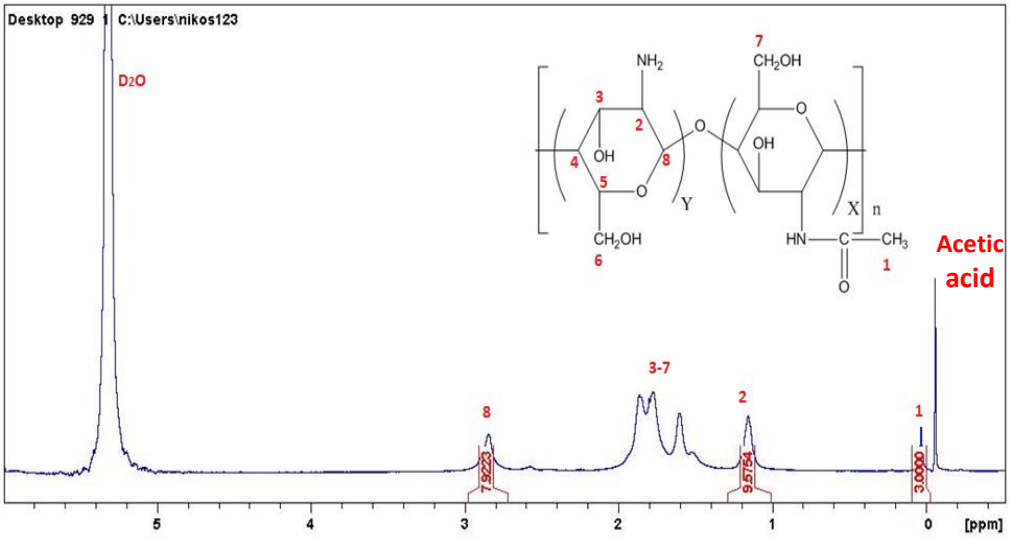

Figure 3.1. ^{1}H NMR spectrum of chitosan at 25 ^{o}C in D_2O.

The degree of deacetylation of chitosan was determined using the integrals of peak 1 (I_1), peak 2 (I_2) and peak 8 (I_8) according to the following equations:

$$DD\ \% = \frac{I_2}{I_2 + \frac{I_1}{3}} \qquad (2)$$

$$DD\ \% = \frac{I_8}{I_8 + \frac{I_1}{3}} \qquad (3)$$

From equation (2) the degree of deacetylation was found:

$$DD\% = \frac{9.5754}{9.5754+1} \simeq 91\ \%$$

Whereas, the degree of deacetylation according to equation (3) was:

$$DD\% = \frac{7.9223}{7.9223 + 1} \simeq 89\ \%$$

Thus, according to the ^{1}H NMR spectrum of chitosan at 25 ^{o}C shown in **Figure 3.1** the degree of deacetylation of chitosan is 90 ± 1 % in good agreement with the specifications provided by the supplier.

In addition, the ^{1}H NMR spectrum of chitosan was acquired at 70 ^{o}C to improve the solubility of the polysaccharide in the acidic medium and is shown in **Figure 3.2**. In this case, the peaks were sharper and better separated compared to the spectrum at 25 ^{o}C.

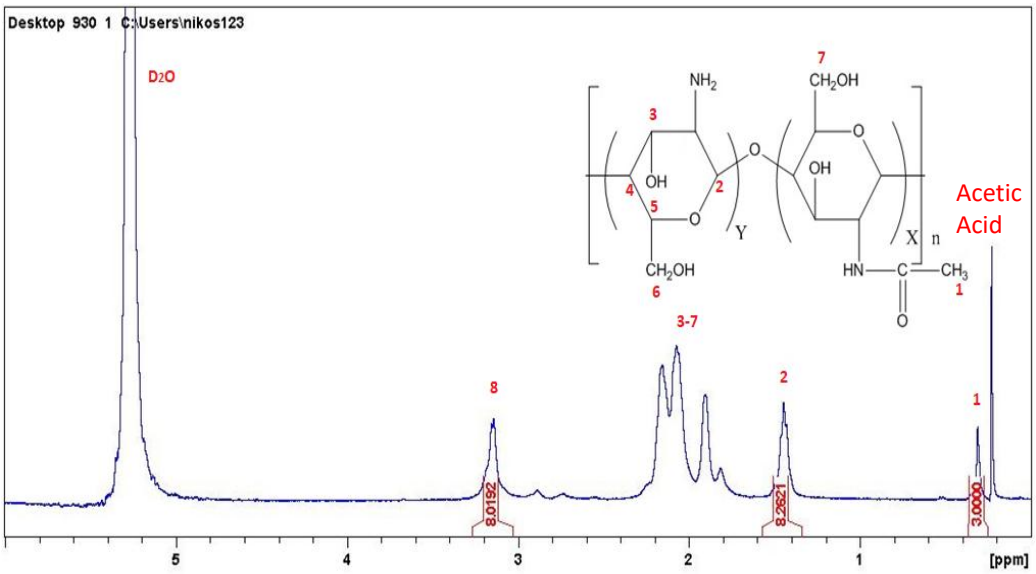

Figure 3.2. ^{1}H NMR spectrum of chitosan at 70 ^{o}C in D_2O.

Again, the integrals of the peaks 1, 2 and 8 were used for the quantification of the degree of deacetylation. The degree of deacetylation of chitosan according to equation (2) was found:

$$DD\% = \frac{8.2621}{8.2621 + 1} \simeq 89\ \%$$

And the degree of deacetylation according to equation (3) was:

$$DD\% = \frac{8.0192}{8.0192 + 1} \simeq 89\ \%$$

In conclusion, the degree of deacetylation of chitosan from its ^{1}H NMR spectrum at 70 ^{o}C was found 89 % in good agreement with the value found by ^{1}H NMR at 25 ^{o}C and the nominal value.[45]

The modified CS was also characterized by ^{1}H NMR spectroscopy, however the spectrum cannot be shown here. The spectrum of modified chitosan verified the successful modification of the polymer.[46]

3.1.2. FTIR characterization of chitosan and modified chitosan

The FTIR spectra of chitosan and modified chitosan are shown in **Figure 3.3**. The spectrum of chitosan (a) reveals a number of characteristic peaks. The peaks at 3344 and 3280 cm^{-1} are attributed to the stretching vibrations of the N-H and O-H bonds respectively. Furthermore, the peaks at 2900 and 2866 cm^{-1} are ascribed to the symmetric and asymmetric stretching vibrations of the C-H bonds. The peaks at 1646 cm^{-1} and 1589 cm^{-1} are attributed to the stretching C=O and N-H vibrations of the primary amine groups, respectively. In addition, the stretching vibration of the CH_2 bonds and the symmetric deformation of the CH_3 bonds are represented by the peaks 1417 and 1375 cm^{-1}, respectively. The C-N stretching vibration of the N-acetyl group is seen in the peak at 1321 cm^{-1}, and the asymmetric stretch of the C-O-C bonds linking the two consecutive sugar repeat units are presented at 1148 cm^{-1}. Finally, the peaks at 1057 and 1026 cm^{-1} are attributed to the C-O stretching vibrations.[47]

Regarding modified chitosan, a new intensive peak can be seen at 1470 cm^{-1} which is attributed to the C-H bending vibrations of CH_2 of the trimethylammonium which according to the literature verifies the modification of chitosan and the addition of the permanent positive charges. Then, the intensity of N-H of the primary amine group at 1589 cm^{-1} in chitosan appears to be weaken in the case of modified chitosan. This can imply that the reaction for the modification of chitosan took place in the amine group.[46]

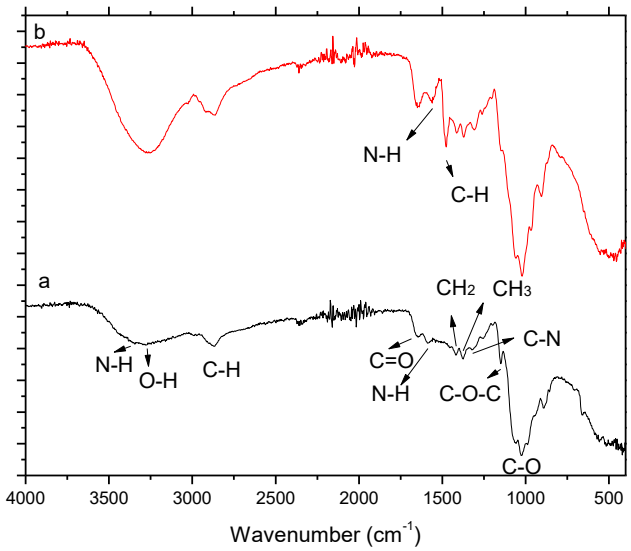

Figure 3.3. FTIR spectra of chitosan (a) and modified chitosan (b).

3.1.3. Thermal properties of chitosan and modified chitosan

CS and modified CS were subsequently characterized by TGA and DSC to investigate their thermal properties. **Figure 3.4** shows the TGA curves of CS and modified CS, while **Figures 3.5** and **3.6** show the 1st derivative of the two curves, respectively.

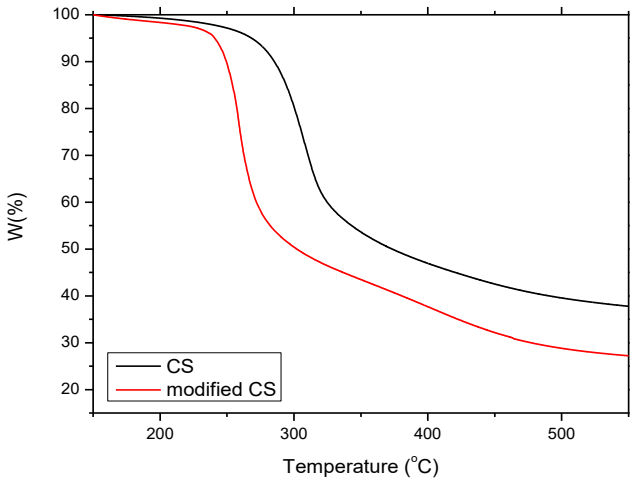

Figure 3.4. TGA curves of CS and modified CS.

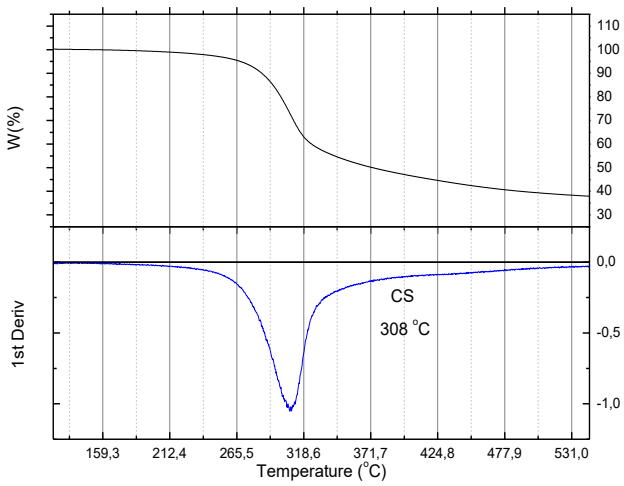

Figure 3.5. 1st derivative of the CS curve.

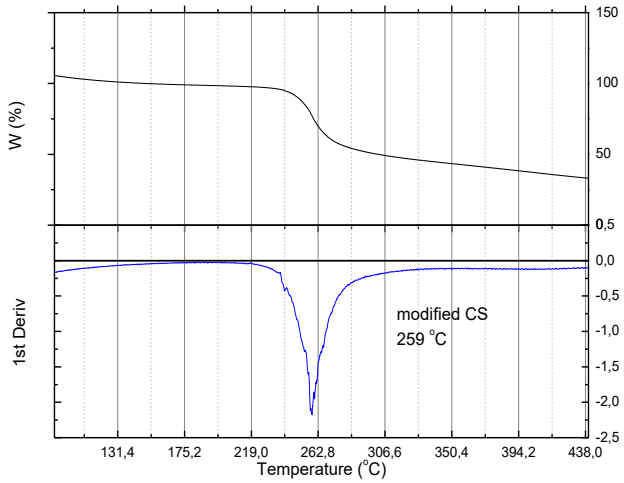

Figure 3.6. 1st derivative of the modified CS curve.

From **Figure 3.4** it can be observed that at 550 °C, 62 % of the original weight of chitosan is lost, while for the case of the modified chitosan, the weight loss is 73 %. The 11% difference can be attributed to the modification that conferred additional organic mass to the modified chitosan. Taking into consideration that the experiments took place under an inert N_2 atmosphere, the remaining mass in both cases is attributed to graphite the crystalline carbon. The latter would not be present under air atmosphere as oxidative reactions would take place leading to CO_2 production.

It is worth noting that the biopolymers differ regarding their maximum decomposition temperature. As shown in **Figure 3.5** the maximum decomposition temperature of CS is 308 °C while in **Figure 3.6** for modified CS it is 259 °C. Since, modified CS is derived from modification of CS, it can be concluded that the modification resulted in poorer thermal stability.

Moreover, **Figures 3.7** and **3.8** shows the heating and cooling cycles respectively of chitosan and modified chitosan.

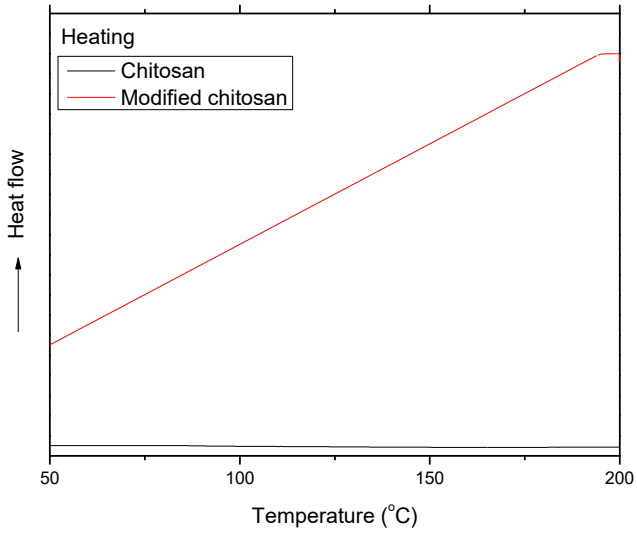

Figure 3.7. DSC curves (heating cycle) of chitosan and modified chitosan.

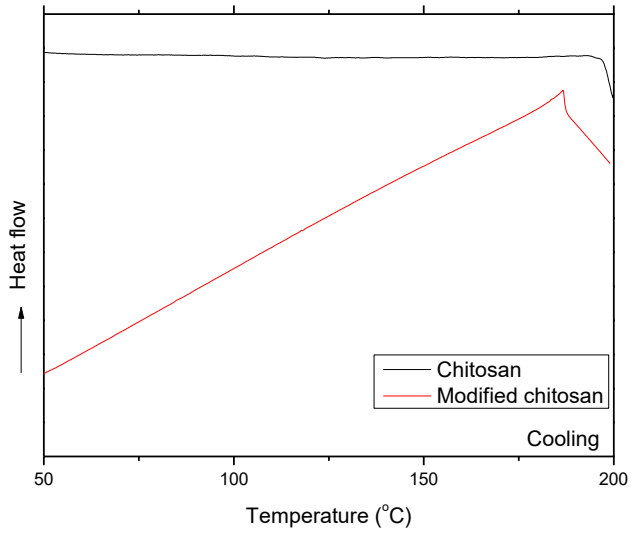

Figure 3.8. DSC curves (cooling cycle) of chitosan and modified chitosan.

Figure 3.7 shows the curves of the heating cycle for chitosan and modified chitosan. The curve representing chitosan does not show any thermal transition in the range between 50 and 200 °C even though it is a semi crystalline polymer. This is because the polymer decomposes at a lower temperature than its melting temperature. The same applies for the case of modified chitosan, where its curve does not reveal any thermal transition.

Figure 3.8 shows the curves of the cooling cycle for chitosan and modified chitosan. Again, no thermal transitions are spotted in both cases.

3.2. Characterization of the PE films before and after oxygen plasma treatment

The coating of the PE substrates with chitosan and its derivative required the activation of the inert, non-polar and hydrophobic PE surface, which was performed by oxygen plasma treatment. Specifically, oxygen plasma treatment cleaves the C-H bonds and results in the formation of functional groups containing oxygen atoms, such as carbonyl, carboxyl and hydroxyl groups, on the polymer treated surface.

The PE films were characterized by FTIR, WCA measurements and FESEM before the plasma treatment and by WCA and FESEM after the plasma treatment.

3.2.1. FTIR characterization of the PE films

Figure 3.9. illustrates the FTIR spectrum of commercial PE. The spectrum shown in **Figure 3.9** reveals the four intensive characteristic peaks of polyethylene[48]. Specifically, the peaks at 2912 and 2834 cm^{-1} are attributed to the asymmetric and symmetric stretching vibrations of C-H. The peak at 1456 cm^{-1} is due to the bending C-H vibration and finally the rocking C-H vibration is seen at 710 cm^{-1}.

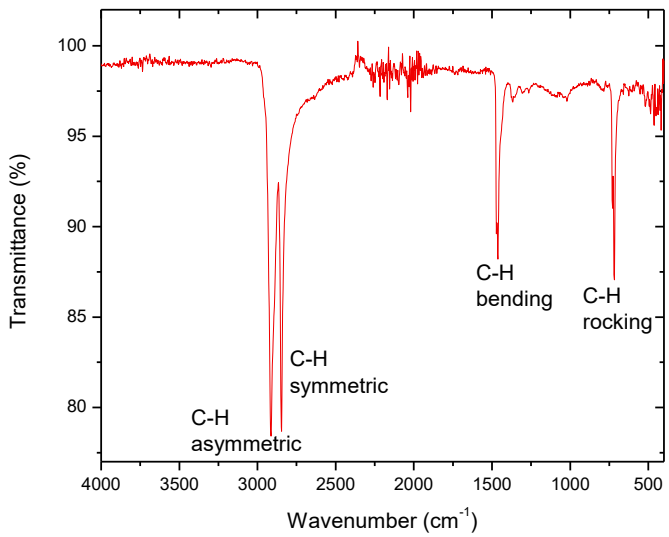

Figure 3.9. FTIR spectrum of commercial PE.

3.2.1. WCA characterization of the PE surface

Oxygen plasma treated PE substrates were prepared for static water contact angle measurements. It has been extensively described in the literature that oxygen plasma has an aging effect and the activation of the surface can be undone as a function of time, as a result of the reorientation of the polar groups into the bulk of the material to attain a lower surface energy. Therefore, it was interesting to investigate the variation in the hydrophilicity of the surface after 1 h and 1 day plasma treatment using static water contact angle measurements.

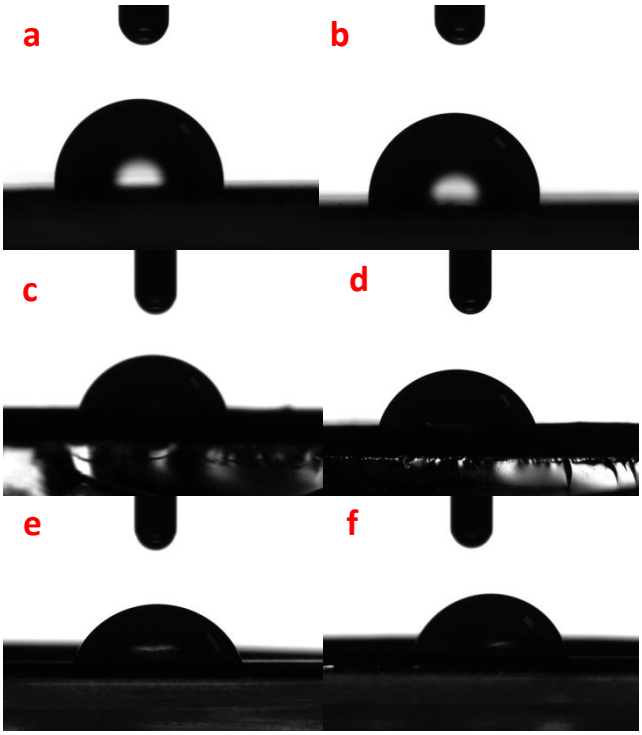

Figure 3.10. WCA measurements of the PE substrates before oxygen plasma treatment (a-b), 1 hour (c-d) and 1 day (e-f) after oxygen plasma treatment.

As shown in **Figure 3.10** the commercial PE film has a WCA of $92^{o} \pm 2^{o}$ which implies its hydrophobicity since the angle is larger than 90°. On the other hand, the oxygen plasma treated polyethylene exhibited a contact angle of $74^{o} \pm 5^{o}$ one hour after plasma treatment, which verified the successful activation of the surface with hydrophilic surface-active groups. One day after the treatment the contact angle was measured $65^{o} \pm 5^{o}$, which suggests that the surface retains its hydrophilicity even after one day treatment, however, in this study the surfaces were used within one hour after plasma treatment to ensure that it is not contaminated due to exposure to the open air.

3.2.2. FESEM characterization of the PE films

Samples of the commercial PE films and the PE films one day after oxygen plasma treatment were characterized by SEM to determine the surface morphology. **Figure 3.11** illustrates the SEM images of the commercial PE substrates (a-b) and the substrates one day after oxygen plasma treatment (c-d).

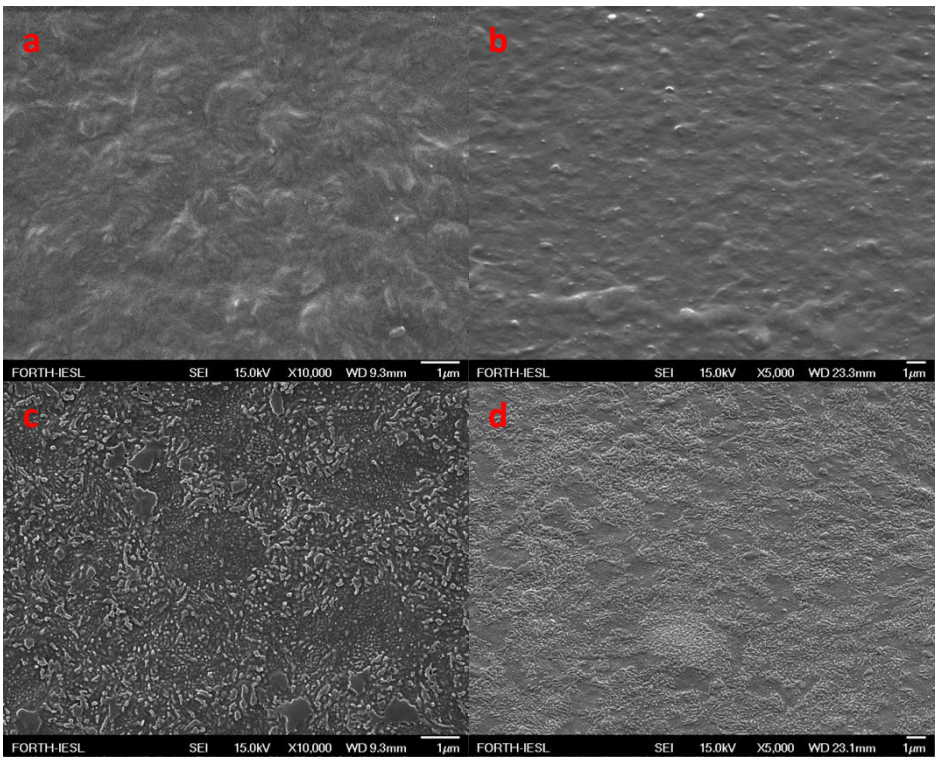

Figure 3.11. FESEM images of commercial PE (a-b) and PE one day after oxygen plasma treatment (c-d).

From the FESEM images, the surface of commercial PE appears to be smooth (Figure 3.12 a) but at lower magnifications the surface appears embossed regions (Figure 3.12 b). After the oxygen plasma treatment, the surface morphology changes dramatically to a much rougher one (Figure 3.12 c and d). This is attributed to the etching and reconstruction effect of the plasma treatment according to the literature.[34]

3.3 Crosslinking of Chitosan

The coating of the substrates with chitosan and its derivative for food packaging applications requires the increased stability of the coatings when they are immersed in water and/or acidic water, in which such polysaccharides are soluble. This can be achieved by the development of covalent bonds between the biopolymers chains

and their effective binding onto the substrate. For this purpose, simple bi-functional or multi-functional molecules, namely crosslinkers, are employed.

As shown in **Table 3.1,** two chitosan solutions in water were prepared using two different acetic acid concentrations in water, which can influence the solubility of chitosan and the crosslinking reaction. A crosslinker was added which is confidential and cannot be reported in this thesis. The solutions were left stirring overnight.

Table 3.1. Reagents used for the crosslinking of chitosan (Samples A and B).

	Chitosan A	Chitosan B
Concentration in water (g/ml)	0.05	0.05
Acetic acid (% v/v in water)	6	8
pH	3.9	3.6
Crosslinker/Chitosan molar ratio	0.35	0.35
Temperature (^{o}C)	25	25

As shown in **Figure 3.12**, after overnight stirring at room temperature, the chitosan crosslinking reaction that took place at pH 3.9 led to a gel, while chitosan crosslinking at pH 3.6 did not lead to any change in the solution viscosity.

Figure 3.12. Crosslinking of chitosan at pH 3.9 and 3.6 (samples A and B) after overnight stirring at room temperature.

A similar experiment took place using lower amount of crosslinker and acetic acid. The chitosan solutions were prepared as shown in **Table 3.2**.

Table 3.2. Reagents used for the crosslinking of chitosan (Samples C and D).

	Chitosan C	Chitosan D
Concentration in water (g/ml)	0.05	0.05
Acetic acid (% v/v in water)	2	4
pH	4.9	4.3
Crosslinker/Chitosan molar ratio	0.10	0.10
Temperature (^{o}C)	25	25

As shown in **Figure 3.13**, after overnight stirring at room temperature, chitosan crosslinking took place at pH 4.9 and led to the formation of a gel, whereas chitosan crosslinking at pH 4.3 did not lead to any obvious change in the solution viscosity.

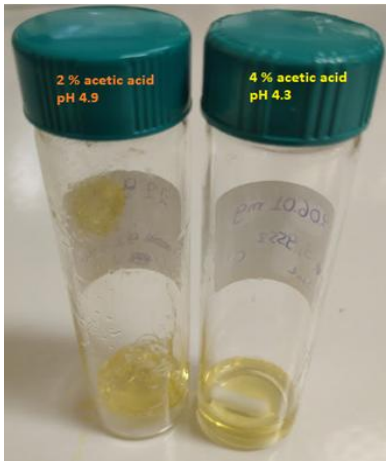

Figure 3.13. Crosslinking of chitosan at pH 4.9 and 4.3 (samples C and D) after overnight stirring at room temperature.

Overall, based on the above results, the pH had a significant influence on the rate of the cross-linking reaction with a more effective gel formation at less acidic environments.

3.4. Antibacterial coatings based on CS and modified CS

The plasma treated PE substrates were coated with CS and modified CS to form the antimicrobial coatings. The latter polymer was used to confer improved solubility in water and enhanced antibacterial properties. For the coating, acidic CS and modified

CS aqueous solutions were prepared and the cross-linker was added in the solutions. **Table 3.3** shows the quantities of the reagents used for the preparation of the solutions. In both cases, CS and modified CS, the water concentration and the crosslinker/CS molar ratio were kept constant. The pH of the solution was adjusted to 4.3 for the modified chitosan and 3.6 for CS, due to the insolubility of the latter at higher pH values.

Table 3.3. Reagents used for the preparation of the polymer solutions coated onto the PE films.

	CS	Modified CS
Concentration in water (g/ml)	0.05	0.05
Acetic acid (% v/v in water)	8	1
pH	3.6	4.3
Crosslinker/Chitosan molar ratio	0.35	0.35
Temperature (^{o}C)	25	25

The coatings were formed onto the plasma treated PE films using the Mayer rods and were left overnight to dry under air. Next, the samples were immersed in acidic water (for CS coatings) and neutral water (for modified CS coatings) to determine the stability of the coatings with immersion time. Samples were also prepared to investigate the barrier, mechanical, thermal and antimicrobial properties of the packaging material before and after coating.

3.4.1. Stability of the CS and modified CS coatings on PE

In order to investigate the stability of the CS and modified CS coatings on the PE substrate, the coated substrates were immersed in acidic and neutral water, respectively. First, FESEM cross-section images of the uncoated PE and the as prepared coated PE were obtained. **Figure 3.14** illustrates cross section FESEM images of the commercial PE substrate. The average thickness of the substrate was

measured 105 ± 3 µm by FESEM (see **Figure 3.14 c**). This is in good agreement with the thickness indicated by the supplier (110 ± 10 µm).

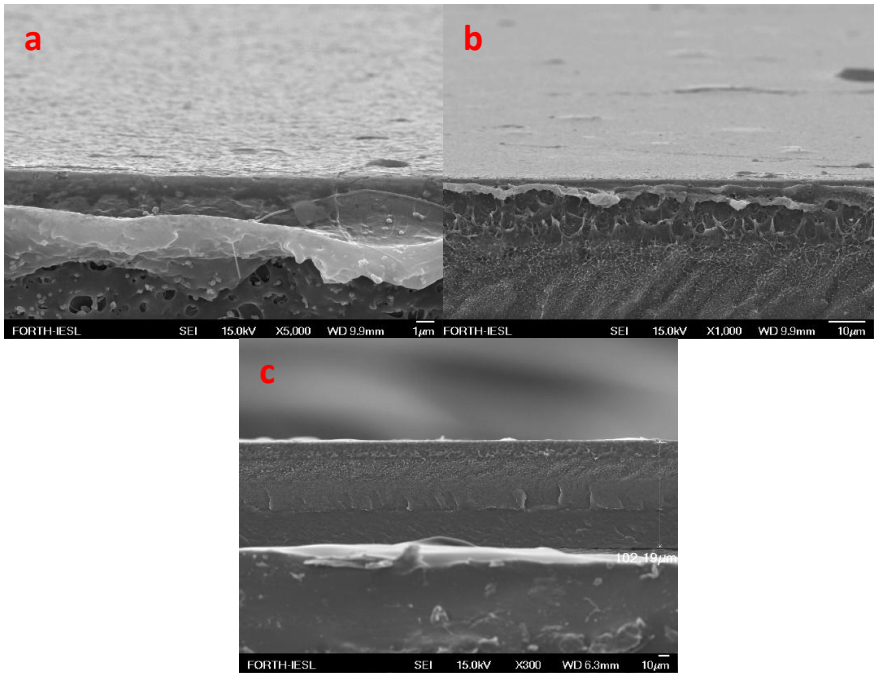

Figure 3.14. Cross section FESEM images of commercial uncoated PE substrates.

Figure 3.15 shows the cross-section FESEM images of the CS and modified CS coated PE films. The CS coating was measured 2.04 ± 0.05 µm by FESEM (**Figure 3.15 a**). After 3 weeks immersion in acidic water (pH 4) a thickness of 3.30 ± 0.04 µm was measured which decreased to 1.31 ± 0.04 µm after 1 month (**Figures 3.15 b** and **c**). The observed increase in the coating thickness of the as prepared PE-CS coating (2.04 µm) and after 3 weeks immersion in water (3.30 µm) can be attributed to the fact that coating was prepared using a metering rod. This manual handling process does not allow to fully control the coating thickness across the substrate and 1 µm thickness variation is possible.

Similarly, the modified CS coating before immersion in water had a thickness of 3.05 ± 0.04 µm (**Figure 3.15 d**), which decreased to 1.35 ± 0.05 µm after two days immersion in water and then remained constant (1.27 ± 0.19 µm) for one month (**Figures 3.15 e** and **f**).

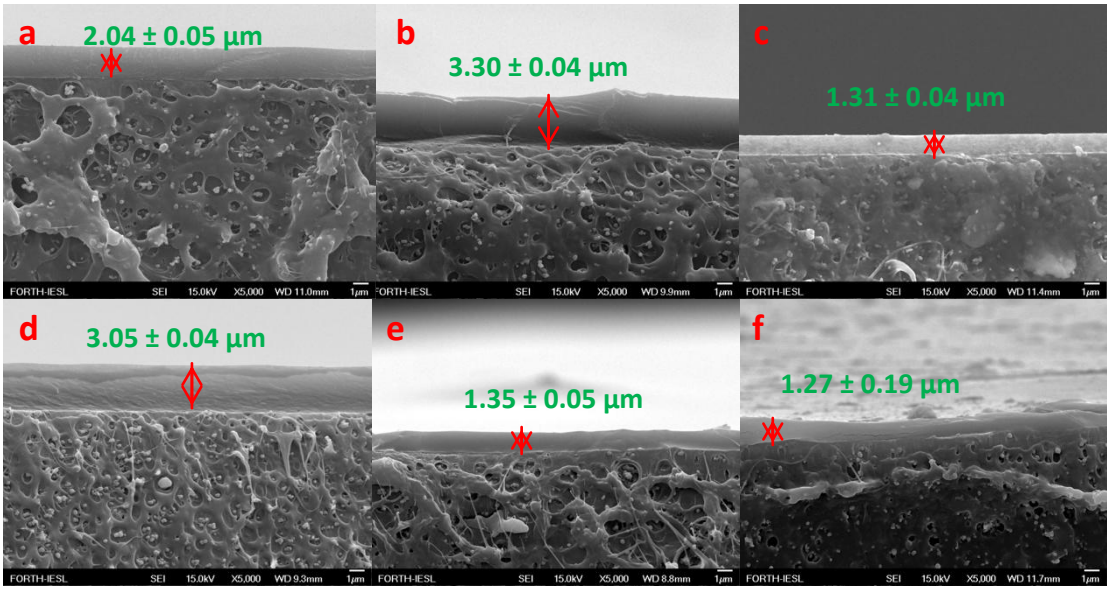

Figure 3.15. Cross section FESEM images of the PE-CS coating (a), the PE-CS coating after 3 weeks (b), and after 1 month (c) immersion in acidic water, the PE-modified CS coating (d), the PE-modified CS coating after overnight (e) and after 1 month (f) immersion in water.

FTIR spectroscopy was also employed to verify the stability of the coatings. **Figure 3.16** shows the spectra at 3 different regions of the PE-CS coating (PE-CS 1, PE-CS 2 and PE-CS 3) in comparison to the spectrum of CS and the commercial PE substrate.

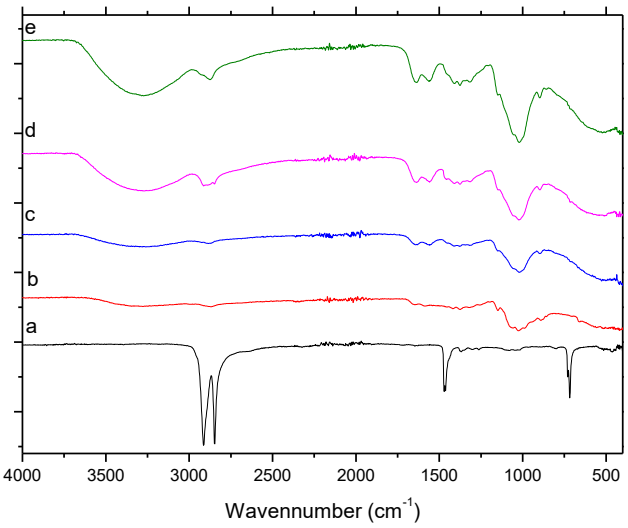

Figure 3.16. FIIR spectra of commercial PE (a), CS (b) and the PE-CS coating (c-e).

The spectra of the coated film comprise all the characteristic peaks of CS verifying the presence of the coating on the substrate. In addition, **Figure 3.17** shows the spectra of the coated film at 3 regions after immersion in acidic water (pH 4) for 2

weeks. The spectra show again all the characteristic peaks which are attributed to CS and thus prove that the CS coating is still present on the substrate. In addition, a new peak is observed at 1410 cm^{1} (arrow), which is attributed to the hydrogen bonding interactions between the carbonyl C=O and O-H groups of acetic acid which was used to adjust the pH of the water medium in which the coated film was immersed.[49]

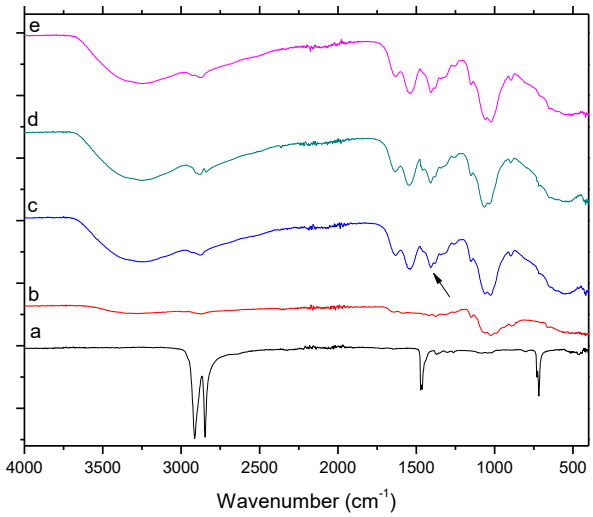

Figure 3.17. FT-IR spectra of commercial PE (a), CS (b) and three regions of the PE-CS coated film after 2 weeks immersion in acidic water (c-e).

FTIR was used to study the stability of the PE-modified CS film. The respective spectra are shown in **Figures 3.18**.

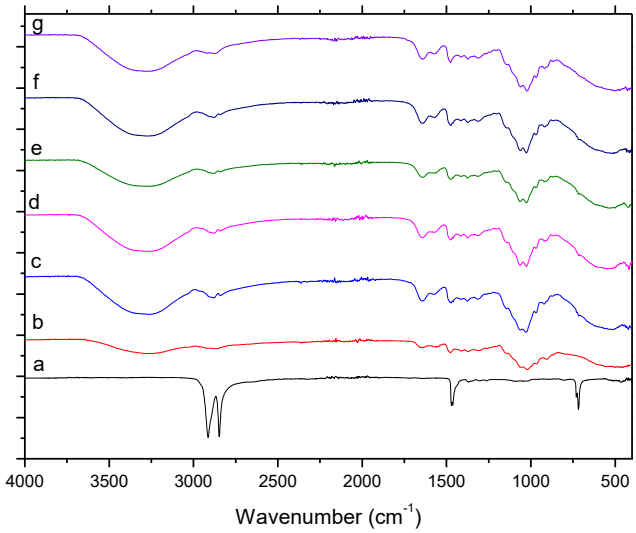

Figure 3.18. FTIR spectra of commercial PE (a), modified CS (b), PE-modified CS coated film (c), two regions of the PE-modified CS film following overnight (d-e) and 1 month (f-g) immersion in water.

It can be observed that both after overnight and after 1 month immersion in water the modified CS is still present on the PE substrates and its characteristic peaks are clearly observed by FTIR.

However, it is worth noting that the protocol used to prepare the modified CS coatings described in **Table 3.3** was not reproducible. Modified CS coatings prepared using different batches of modified CS to coat the PE substrates were not always homogeneous and would form patches onto the substrate.

To solve this problem, we decided to add less acetic acid in the solution, and in particular 0.25 v/v % acetic acid in water (pH 5.2) was added. The modified CS coated the substrates homogeneously, while cross section FESEM images proved the formation of reproducible PE-modified CS coatings before and after overnight and 1 month immersion in water (see **Figure 3.19**).

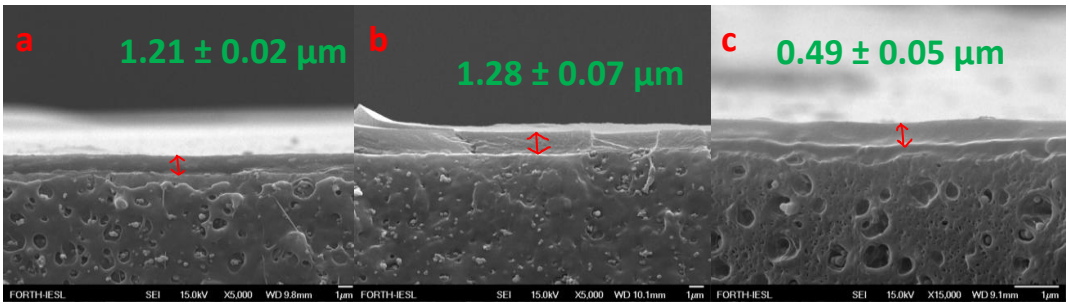

Figure 3.19. Cross section FESEM images of PE-modified CS coatings prepared with 0.25 v/v % acetic acid (a), after overnight (b) and after 1 month (c) immersion in water.

FESEM images verified that after overnight and after 1 month immersion in water the modified CS coating was still present on the PE substrates with a 1.28 ± 0.07 µm and 0.49 ± 0.05 µm thickness, respectively.

Moreover, FTIR spectroscopy verified the presence of modified CS on the substrates after 1 week, 2 weeks and 1 month immersion in water with all the characteristic modified CS peaks appearing in the spectra shown in **Figures 3.20** and **3.21**.

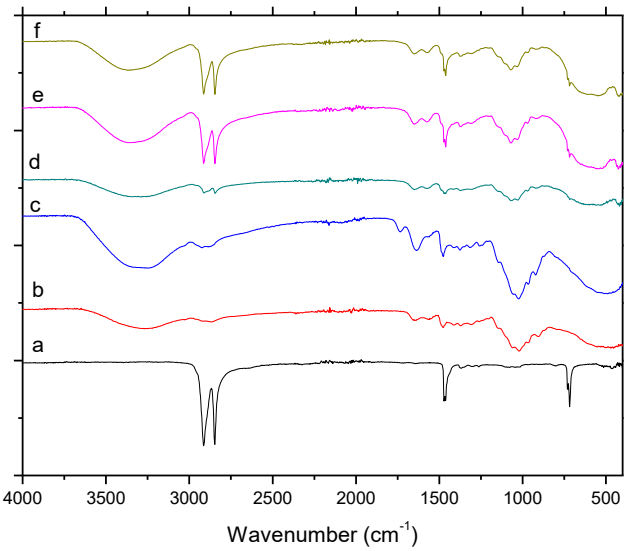

Figure 3.20. FTIR spectra of commercial PE (a), modified CS (b), PE-modified CS coating (c) and three regions on the PE-modified CS coating after 1 week immersion in water (d-f).

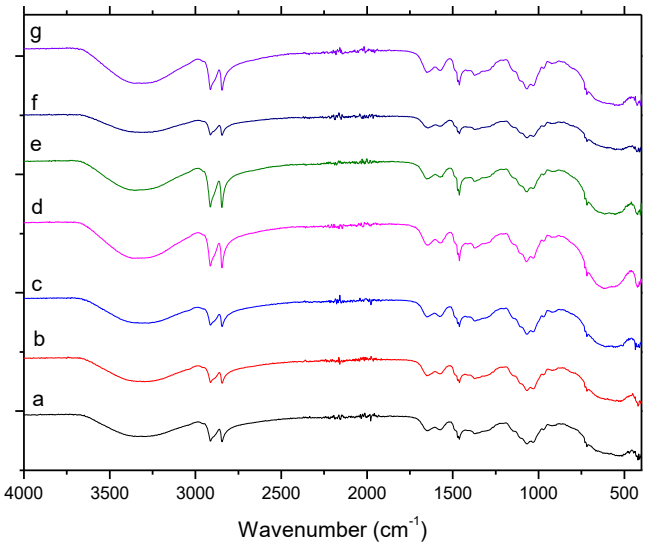

Figure 3.21. FTIR spectra of three regions on the PE-modified CS coatings after 2 weeks immersion in water (a-c) and four regions after 1 month immersion in water (d-g).

The above data suggest that the proposed coatings are stable enough for use in food packaging PE films.

Tables 3.4 and **3.5** shows the influence of the crosslinker content and the solution pH on the stability of the PE-CS and PE-modified CS coatings, respectively.

Table 3.4. Crosslinker content and pH employed for the preparation of the PE-CS coatings.

	Concentration in water (g/ml)	Acetic acid in water (% v/v)	pH	Crosslinker/CS molar ratio	Result
PE-CS	0.05	4	4.3	0.1	Coatings remained stable for at least 2 days in acidic water. After 3 weeks the coating was removed.
PE-CS	0.05	2	4.9	0.2	Fast crosslinking in solution and unstable coating.
PE-CS	0.03	4	3.9	0.2	Coatings were stable for 3 weeks but not after 1 month immersion in acidic water.
PE-CS	0.05	8	3.6	0.35	Stable coatings even after 1 month immersion in water.

Table 3.5. Crosslinker content and pH employed for the preparation of the PE-modified CS coatings.

	Concentration in water (g/ml)	Acetic acid in water (% v/v)	pH	Crosslinker/QCS molar ratio	Result
PE-modified CS	0.05	-	7.6	0.1	After overnight immersion in water the coating was removed in most cases.
PE-modified CS	0.05	1	4.3	0.1	After overnight immersion in water the coating was removed.
PE-modified CS	0.05	1	4.3	0.2 or 0.35	Coatings were stable after 1 month immersion in water. Protocol not reproducible in this pH.
PE-modified CS	0.05	0.25	5.2	0.35	Coatings were stable after 1 month immersion in water. Reproducible protocol.
PE-modified CS	0.05	4	3.6	0.1 or 0.2	Inhomogeneous coatings and removal after immersion in water.
PE-modified CS	0.05	-	7.6	0.35	Fast crosslinking in solution. Coatings were removed after 1 hour immersion in water.

It was found that the crosslinker content and the pH of the solution had a high impact on the stability of the coatings. Regarding the amount of the crosslinker, at a crosslinker/chitosan molar ratio below 0.35 the coatings were removed after immersion in water.

Furthermore, for less acidic CS solutions (i.e., 2 v/v % acetic acid in water (pH 4.9)) a rapid crosslinking of the chitosan solution was observed which led to unstable coatings on the PE substrate. This implied that in less acidic media, crosslinking takes place rapidly between the biopolymer chains, which prevents the effective adhesion of the coating to the substrate. A similar effect was found for the modified CS coatings. It is assumed that at higher pH the amine groups of CS are non-protonated and cross-link rapidly to form a gel.

3.4.2. Barrier properties of the coated PE films

An appropriate food packaging film must comprise adequate barrier properties to protect the food from the outer environment. Samples of commercial PE and coated PE films were studied for their barrier properties against oxygen by measuring the oxygen transmission rate (OTR) under 0 % relative humidity (Rh) at 23 ^{o}C and water vapor by measuring the water vapor transmission rate (WVTR) under 90 % Rh and 38 ^{o}C. The present study was carried out by Hatzopoulos S.A.

The barrier properties of the PE coated films against oxygen were determined by measuring the oxygen transmission rate (OTR) in $\frac{cm^3}{m^2 * 24\ h}$. The results of the study are shown in **Figure 3.22**.

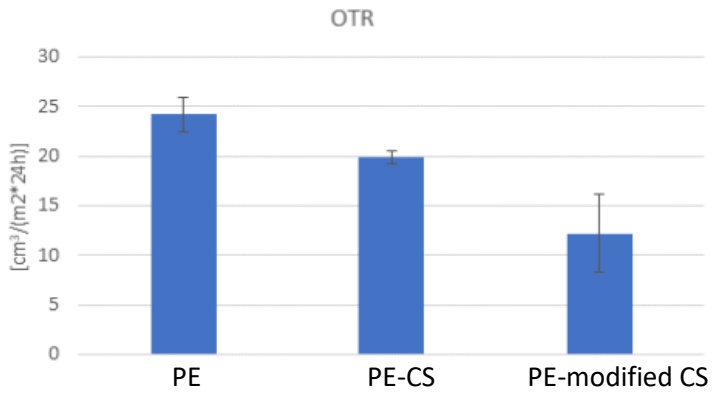

Figure 3.22. OTR of commercial PE, PE-CS and PE-modified CS films.

As shown in **Figure 3.22** the OTR of commercial PE was found 24.213 ± 1.724 $\frac{cm^3}{m^2*24\,h}$. A decrease in the OTR was observed for the PE-CS film at 19.856 ± 0.639 $\frac{cm^3}{m^2*24\,h}$, while for the PE-modified CS coated film, a further decrease at 12.222 ± 3.937 $\frac{cm^3}{m^2*24\,h}$ was found. These results imply that CS coatings with thickness in the micrometer range enhance the barrier properties of the substrates against oxygen, while the PE-modified CS coated films confer the substrates an even more effective barrier.

For the study of the barrier properties of the PE coatings against water vapor, the water vapor transmission rate (WVTR) was measured in $\frac{g}{m^2*day}$. The results of the study are shown in **Figure 3.23**.

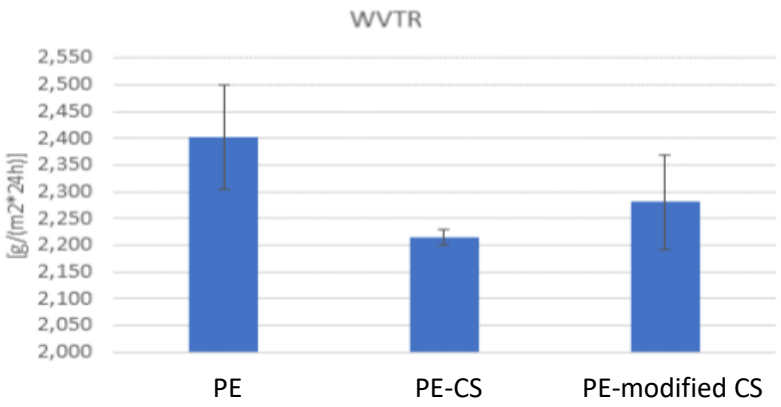

Figure 3.23. WVTR of commercial PE, PE-CS and PE-modified CS films.

As shown in **Figure 3.23** the WVTR of commercial PE was found 2.402 ± 0.098 $\frac{g}{m^2*day}$. A major decrease in the WVTR was observed for the PE-CS film at 2.216 ± 0.015 $\frac{g}{m^2*day}$. Regarding the PE-modified CS coated film, the OTR was measured 2.281 ± 0.088 $\frac{g}{m^2*day}$ which is lower compared to the commercial PE film, but higher that the PE-CS coated film. This can be attributed to the higher hydrophilicity of the modified CS compared to CS, which increases the water permeability.

In conclusion, barrier studies of the commercial PE, PE-CS and PE-modified CS films were carried out against oxygen and water vapor. The results showed that both coatings confer the commercial PE an enhanced barrier against oxygen and water vapor. Therefore, the coatings can be considered as adequate candidates for food packaging applications.

3.4.3. Mechanical Properties of the coated PE films

For the tensile studies, the films were studied in both the machine and transversal direction. PE commercial films were compared with the coated film regarding their strain before sample break (%), the maximum force applied (force at peak in N) and the Young modulus (N/mm^2).

Figures 3.24 and **3.25** illustrate the stress-strain spectra of the commercial PE films in the machine and transversal direction, respectively. From the spectrum in the machine direction the strain before break was found 412.381 ± 29.405 % and the maximum applied force 56.015 ± 4.182 N. Finally, the Young's modulus is calculated 289.323 ± 21.763 N/mm^2. Regarding the transversal direction, the strain before break was 455.034 ± 12.599 %, the maximum applied force 53.873 ± 2.092 N and the Young's modulus 318.116 ± 7.638 N/mm^2.

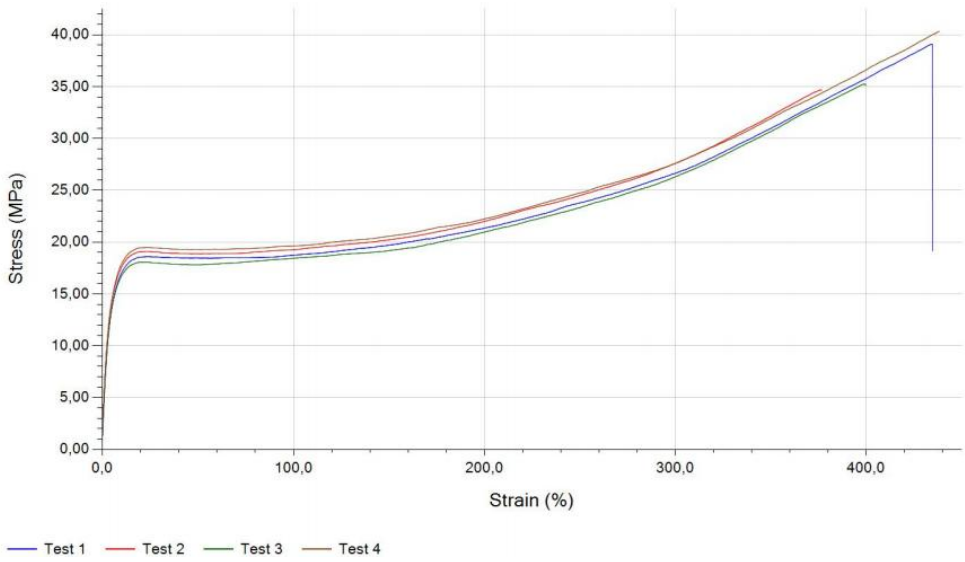

Figure 3.24. Stress-strain curves of commercial PE in the machine direction.

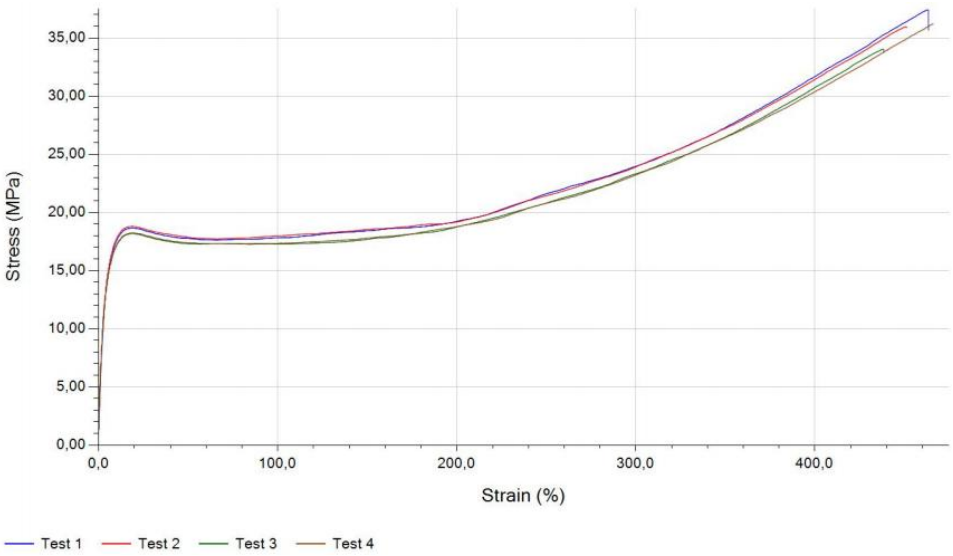

Figure 3.25. Stress-strain curves of commercial PE in the transversal direction.

From these data it can be concluded, that the mechanical properties of commercial PE in the machine and transversal directions exhibit minor differences, given the standard deviation of the measurements.

On the other hand, **Figures 3.26** and **3.27** show the stress-strain spectra of the CS coated PE films in the machine and transversal direction, respectively.

From the curve in the machine direction, the strain before break was found 477.341 ± 18.316 %, the maximum applied force 66.790 ± 4.251 N and the Young modulus 256.239 ± 30.258 N/mm^2.

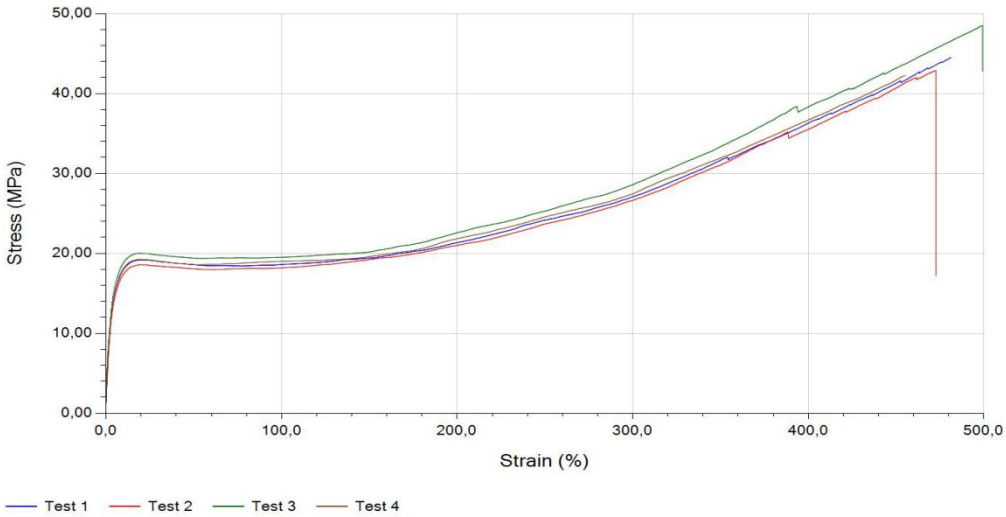

Figure 3.26. Stress-strain curves of the PE-CS coated film in the machine direction.

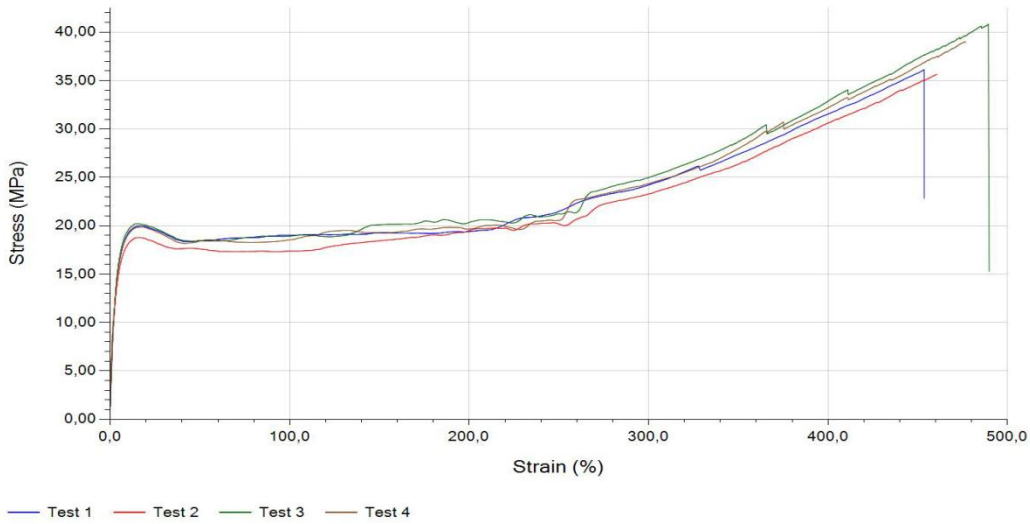

Figure 3.27. Stress-strain curves of the PE-CS coated film in the transversal direction.

In comparison with the mechanical properties of the commercial PE film in the machine direction, an increase in the strain before break can be noted, from 412.381 ± 29.405 % to 477.341 ± 18.316 %. A slight increase in the maximum applied force from 56.015 ± 4.182 N to 66.790 ± 4.251 N is also observed. Finally, regarding the Young's modulus, no difference was found between the two samples, uncoated and CS coated PE, given the standard deviation of the measurements.

Moreover, in the transversal direction the maximum strain before break was found 470.285 ± 16.172 %, the maximum force 56.865 ± 3.672 N and the Young's modulus 339.072 ± 80.888 N/mm^2 for the PE-CS film. In this case, comparison with the transversal direction of the commercial PE film, no significant differences in the mechanical properties were found given the standard deviation of the measurements.

Finally, **Figures 3.28** and **3.29** show the stress-strain spectra of the modified CS coated PE films in the machine and transversal direction, respectively.

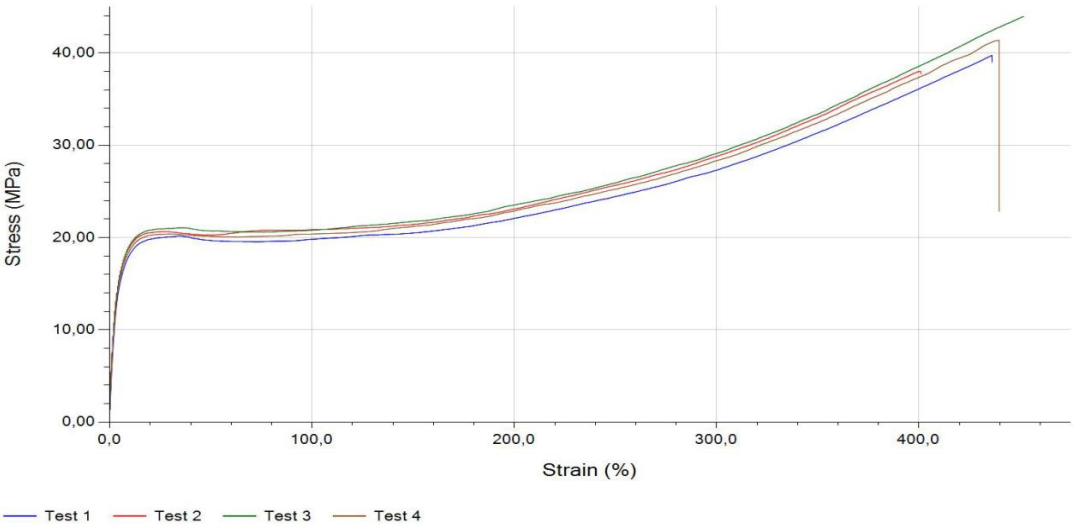

Figure 3.28. Stress-strain curves of the PE-modified CS coated film in the machine direction.

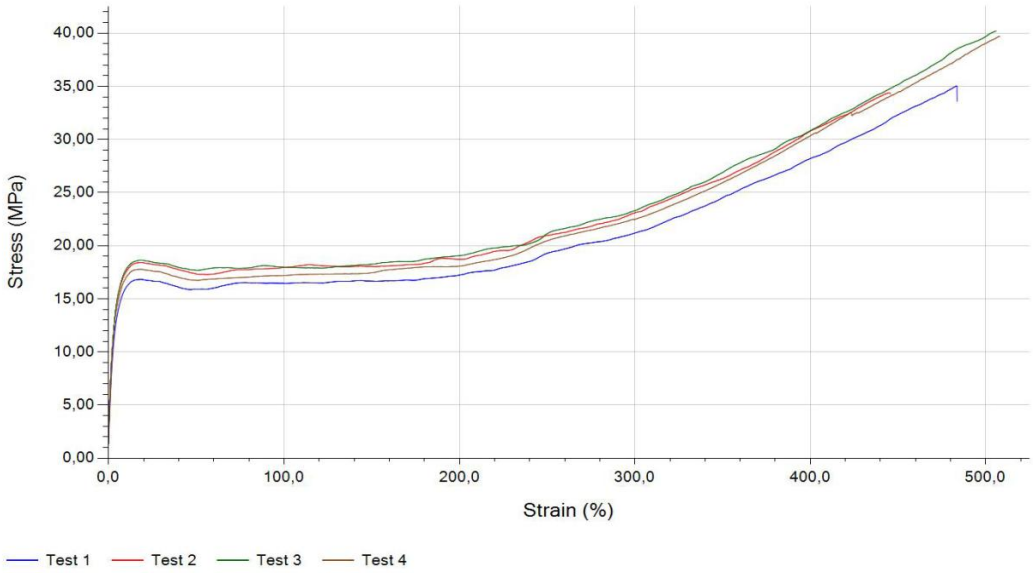

Figure 3.29. Stress-strain curves of the PE-modified CS coated film in the transversal direction.

For this sample, the strain before break in the machine direction (**Figure 3.28**) was found 432.406 ± 21.800 %, the maximum applied force 61.150 ± 3.786 N and the Young's modulus 339.582 ± 17.895 N/mm^2. In comparison with the commercial PE film in the machine direction, an increase in the Young's modulus was observed from 289.323 ± 21.763 to 339.582 ± 17.895 N/mm^2, while in comparison with the PE-CS film in the machine direction, a decrease in the strain before break from 477.341 ± 18.316 % in PE-CS to 432.406 ± 21.800 % and an increase in the Young's modulus from 256 ± 239 N/mm^2 in PE-CS to 339.582 ± 17.895 N/mm^2 was found.

From the curves concerning the transversal direction of the PE-modified CS films (**Figure 3.29**) the strain before break was found 485.034 ± 28.910 %, the maximum applied force 56.000 ± 4.570 N and the Young's modulus 320.408 ± 7.549 N/mm^2.

Comparing the mechanical properties of the PE-modified CS films in the transversal direction to those of the commercial PE and the PE-CS coated films, no significant changes were observed suggesting that the coating does not affect the mechanical properties in this direction of the films.

The mechanical properties of all the films and in all directions are summarized in **Table 3.6**. Overall, the changes in the mechanical properties of the commercial PE film due to the CS and modified CS coatings were observed mainly in the machine direction film. The PE-CS film exhibited a higher strain before break compared to the commercial PE film, whereas, the PE-modified CS films showed an increased Young's modulus compared to the precursor PE film and the Cs coated film. It is worth noting that a material with higher Young's modulus requires a larger force for deformation and becomes stiffer. The above results of the mechanical properties of the coated film suggest that the proposed coatings are appropriate candidates for industrial use.

Table 3.6. Mechanical properties of the PE film before and after the coating with CS and modified CS in the machine and transversal direction.

	PE transversal	PE-CS Transversal	PE-modified CS transversal	PE machine	PE-CS machine	PE-modified CS machine
Strain at break (%)	455.034 ± 12.599	470.285 ± 16.172	485.969± 28.910	412.381 ± 29.405	477.341 ± 18.316	432.406 ± 21.800
Force at peak (N)	53.873 ± 2.092	56.865 ± 3.672	56.000 ± 4.570	56.015 ± 4.182	66.790 ± 4.251	61.150± 3.786
Young modulus (N/mm^2)	318.116 ±7.638	339.072 ± 80.888	320.408 ±7.549	289.323 ± 21.763	256.239 ± 30.258	339.582 ± 17.895

3.4.4. Thermal Properties of the coated PE films

The thermal properties of the commercial PE film before after coating were studied by TGA and DSC.

The TGA curves of commercial PE, and the PE-CS and PE-modified CS coated films are shown in **Figure 3.30**. The first derivatives of the curves are shown in **Figures 3.31**, **3.32** and **3.33,** respectively.

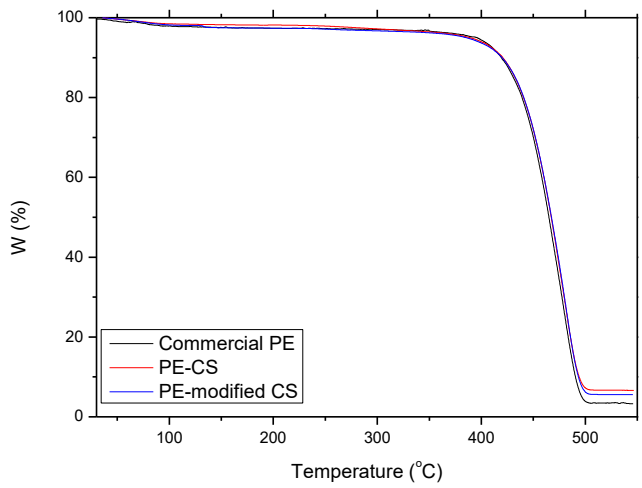

Figure 3.30. TGA curves of the commercial PE, PE-CS and PE-modified CS films.

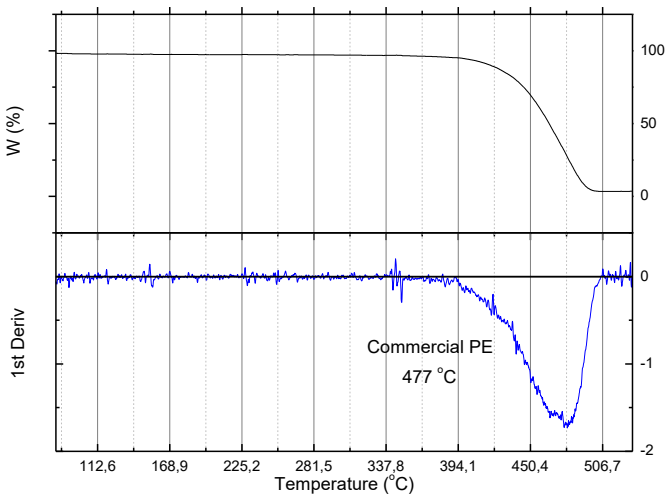

Figure 3.31. 1st derivative of the TGA curve of the commercial PE film.

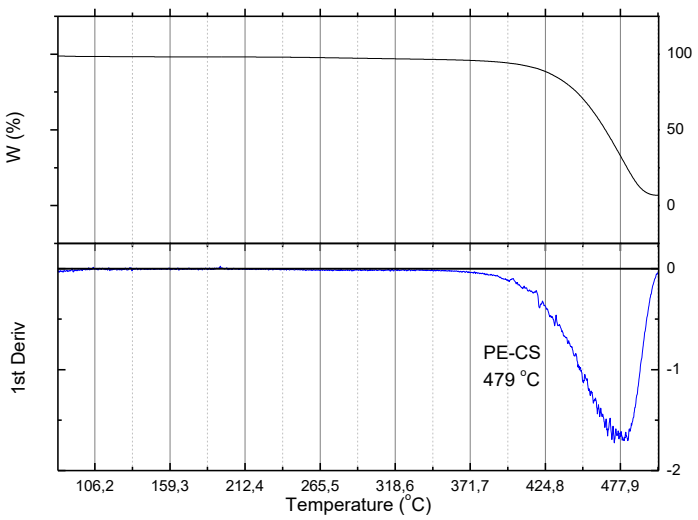

Figure 3.32. 1st derivative of the TGA curve of the PE-CS film.

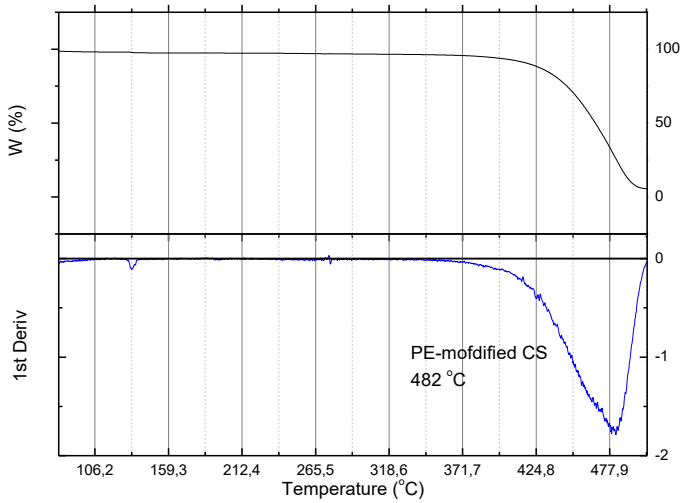

Figure 3.33. 1st derivative of the TGA curve of the PE-modified CS film.

The TGA curves in **Figure 3.30** showed that at 550 °C the weight loss for the commercial PE film was 97 %, for PE-CS 95 % and for PE-modified CS 94 %. Moreover, **Figures 3.31** to **3.33** show that the maximum decomposition temperature of commercial PE is 477 °C, while for PE-CS and PE-modified CS the respective temperature was found 479 °C and 482 °C, respectively. Given the error bars in the TGA measurements, no significant differences regarding the thermal decomposition of the films were found with the commercial PE decomposing at a similar rate and temperature to the CS and modified CS films.

Next, the films were characterized by DSC. **Figures 3.34** and **3.35** show DSC curves of the heating and cooling cycle respectively regarding the commercial PE, PE-CS compared to the curve of CS.

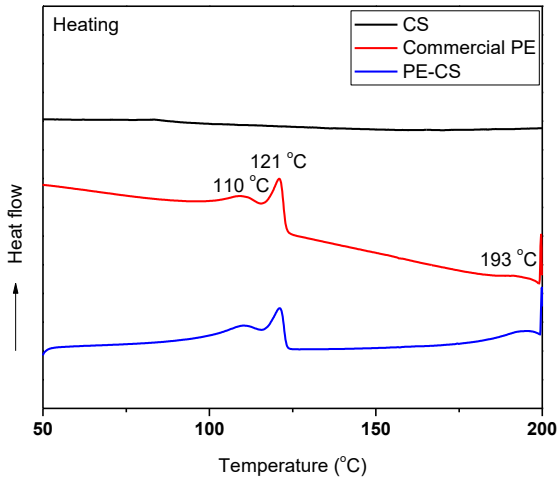

Figure 3.34. DSC curves (heating cycle) of CS, and the commercial PE and PE-CS films.

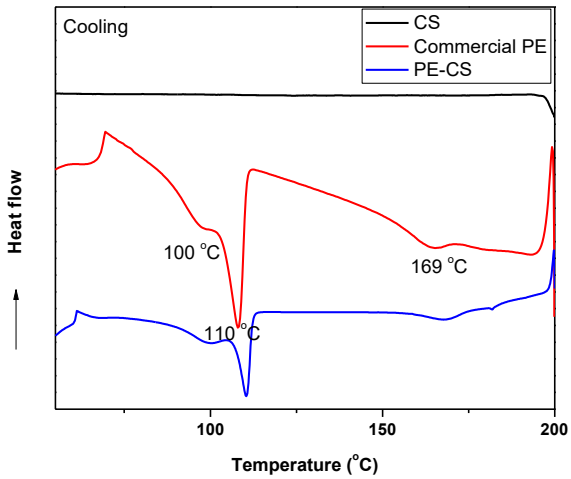

Figure 3.35. DSC curves (cooling cycle) of CS, and the commercial PE and PE-CS films.

As shown in **Figure 3.34**, the curve attributed to chitosan does not show any thermal transition from 50 to 200 °C as it was previously mentioned. On the other hand, the curve of commercial PE exhibits three peaks. The first at 110 °C is attributed to the melting point of low-density polyethylene. The second one at 121 °C is attributed to the melting point of the linear low-density polyethylene and the third one at 193 °C is attributed to the melting point of the polyamide layer. Similar peaks were observed in the DSC thermograms of the CS coated PE film, suggesting that the coating does not have any effect on the thermal transitions of the films.

Similar, as shown in **Figure 3.35**, no transitions were found in the cooling cycle for CS, while the commercial PE films exhibited again three peaks, the first at 100 °C, attributed to the crystallization temperature of LDPE, the second at 110 °C corresponding to the crystallization temperature of LLDPE and the third at 169 °C attributed to the crystallization temperature of the polyamide layer. Similar transitions were observed in the cooling cycle of the DSC thermograms of the CS coated PE film in good agreement with the results above.[50-52]

Next the modified chitosan coated PE films were characterized by DSC, **Figures 3.36** and **3.37** show the DSC curves of the heating and cooling cycle respectively attributed to the commercial PE and PE- modified CS compared to the curve of modified CS.

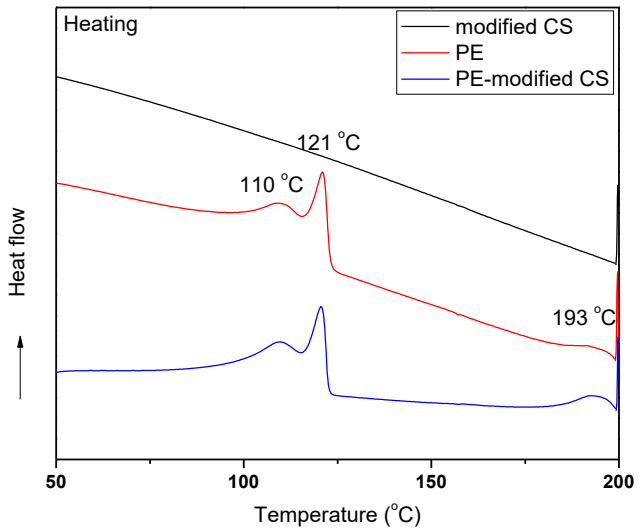

Figure 3.36. DSC curves (heating cycle) of modified CS, commercial PE and PE-modified CS.

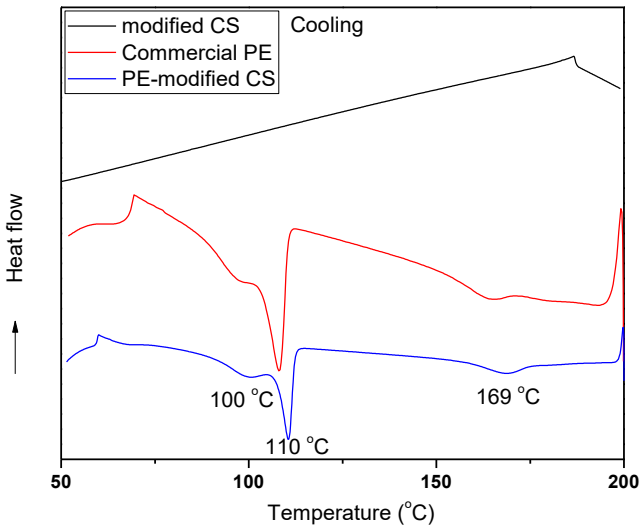

Figure 3.37. DSC curves (cooling cycle) of modified CS, commercial PE and PE-modified CS.

Similar to the chitosan coated films, the six characteristic peaks of the commercial PE film, three in each of the heating and cooling cycles, appeared, but no transition due to the modified CS coating are observed. Therefore, the coatings on the PE films do not present any thermal transitions in this temperature range and also do not affect the melting and crystallization transitions of the commercial PE substrates. **Table 3.7** summarizes the thermal properties of CS, modified CS, and the commercial PE, PE-CS and PE-modified CS films.

Table 3.7. Thermal properties of CS, modified CS, and the commercial PE, PE-CS and PE-modified CS films.

	Weight loss at 550 °C (%)	Maximum Decomposition Temperature (°C)	T_m	T_c
CS	62	308	-	-
Modified CS	73	259	-	-
PE	97	477	110 (LDPE) 121(LLDPE) 193 (PA)	100 (LDPE) 110 (LLDPE) 169 (PA)
PE-CS	95	479	110 (LDPE) 121(LLDPE) 193 (PA)	100 (LDPE) 110 (LLDPE) 169 (PA)
PE-modified CS	94	482	110 (LDPE) 121(LLDPE) 193 (PA)	100 (LDPE) 110 (LLDPE) 169 (PA)

3.5. Antimicrobial activity of the coated PE films

Regarding the antimicrobial study which was carried out by Eleni Ouranou (School of Medicine, University of Crete), *S. aureus*, *E. coli* and *L. monocytogenes* were employed for evaluating the antibacterial properties of the CS and modified CS coated PE films, which were compared to the commercial PE film.

Figure 3.38 shows the initial population of *S. aureus* strains on the commercial PE film (blue bar) at t = 0 and t = 24 h. A one log reduction in the bacteria population on the film is observed after 24 h incubation (orange bar). Furthermore, 1 log reduction can be also observed after 24 h on the PE-CS films (grey bar), while finally the PE-modified CS films exhibited almost complete cell death with ~4.5log reduction after 24 h on the bacteria population (yellow bar).

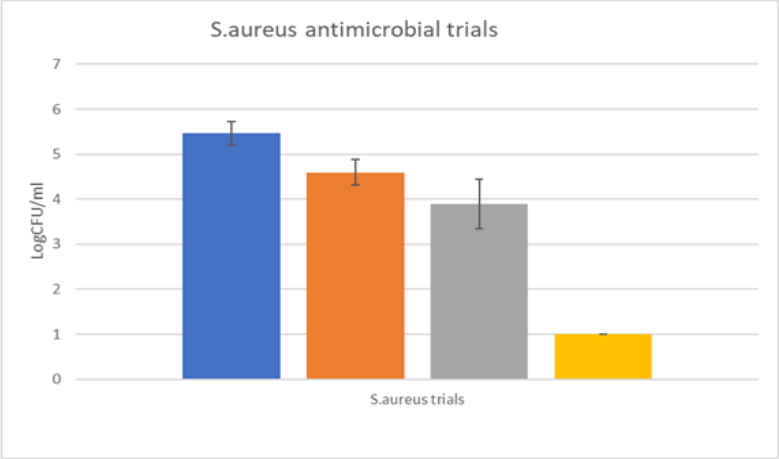

Figure 3.38. *S. aureus* population on commercial PE films at t = 0 (blue bar) and t = 24 h (orange bar) and the PE-CS films (grey bar), PE-modified CS films (yellow bar) at t = 24 h.

Moreover, the average antimicrobial activity R of the PE-CS and PE-modified CS films against *S. aureus* was calculated 0.21 ± 0.13 and 3.87 ± 0.29, respectively as shown in **Tables 3.8** and **3.9**.

Table 3.8. Antimicrobial activity R of PE-CS films against *S. aureus*.

PE-CS	Antimicrobial Activity, R
S. aureus	0.336007579
	0.299002609
	0
	0.208276
Average R	**0.210821533 ± 0.130288**

Table 3.9. Antimicrobial activity R of PE-modified CS films against *S. aureus*.

PE-modified CS	Antimicrobial Activity, R
S. aureus	3.419129308
	4.19266036
	4.034762106
	3.817069316
Average R	**3.865905273 ± 0.290377**

Subsequently, **Figure 3.39** shows the initial population of *E. coli* on commercial PE (blue bar), foe which less than 1 log reduction is observed for both the commercial PE film after 24 h incubation (orange bar) and for the PE-CS films (grey bar). Finally, regarding the PE-modified CS films, a further 2 log reduction is observed after 24 h (yellow bar). It is worth noting that some films exhibited complete cell death, while in other samples a few living cells where observed, which led to the large error bar in the measurements.

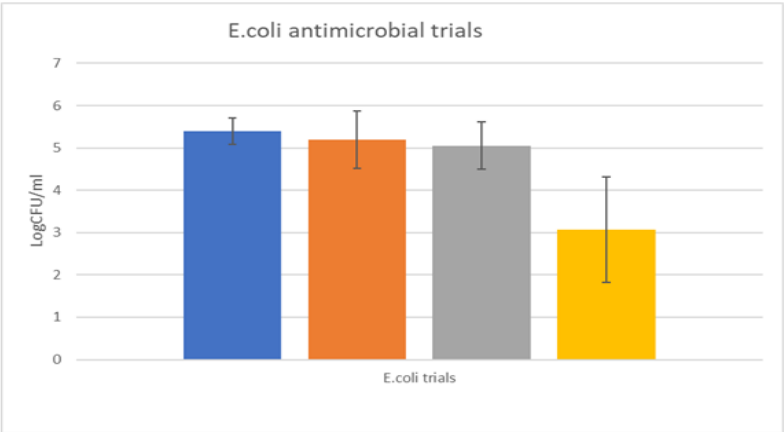

Figure 3.39. *E. coli* population on commercial PE films at t = 0 (blue bar) and t = 24 h (orange bar) and the PE-CS films (grey bar), PE-modified CS films (yellow bar) at t = 24 h.

The antimicrobial activity R calculated for the PE-CS and PE-modified CS films against *E. coli* was found 0.23 ± 0.18 and 0.73 ± 0.33, respectively as shown in **Tables 3.10** and **3.11**.

Table 3.10. Antimicrobial activity R of PE-CS films against *E. coli*.

PE-CS	Antimicrobial Activity, R
E. coli	0.0661403
	0.189634761
	0.553638109
	0.237761741
	0.349967919
	0
	0.0661403
Average R	**0.232857138 ± 0.182813**

Table 3.11. Antimicrobial activity R of PE-modified CS films against *E. coli*.

PE-modified CS	Antimicrobial Activity, R
E. coli	0.610303965
	0.431850254
	1.388291372
	0.705130313
	0.391956927
	0.82596
Average R	**0.7261886 ± 0.331987**

Finally, antimicrobial studies of the *L. monocytogenes* strains on commercial PE, PE-CS and PE-modified CS films were conducted and the results are shown in **Figure 3.40**. The initial population on commercial PE (blue bar) did not exhibit any significant reduction after 24 h incubation (orange bar), while for the case of the PE-CS films, a 1 log reduction is observed after 24 h (grey bar), which increases to 1.5 log reduction for the PE-modified CS films after 24 h (yellow bar).

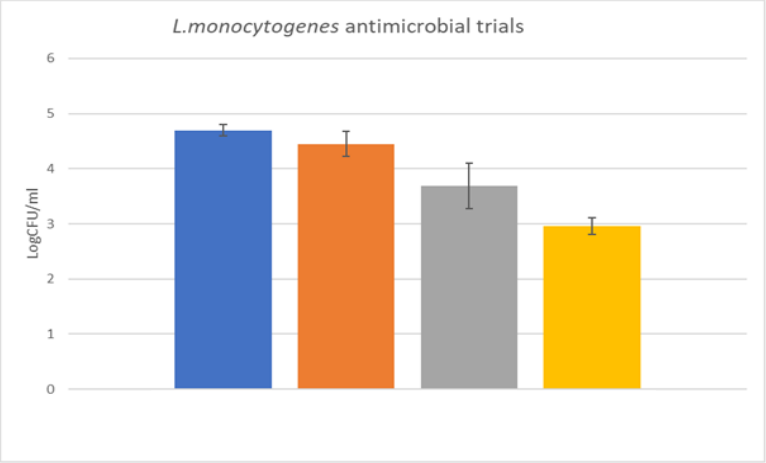

Figure 3.40. *L. monocytogenes* population on commercial PE films at t = 0 (blue bar) and t = 24 h (orange bar) and the PE-CS films (grey bar), PE-modified CS films (yellow bar) at t = 24 h.

The antimicrobial activity R of the PE-CS and PE-modified CS films against *L. monocytogenes* was calculated 0.00068 ± 0.00068 and 0.30 ± 0.20, respectively as shown in **Tables 3.12** and **3.13**

Table 3.12. Antimicrobial activity R of PE-CS films against *L. monocytogenes*.

PE-CS	Antimicrobial Activity, R
L. monocytogenes	0.001356747
	0
Average R	**0.000678374 ± 0.000678**

Table 3.13. Antimicrobial activity R of PE-modified CS films against *L. monocytogenes*.

PE-modified CS	Antimicrobial Activity, R
L. monocytogenes	0.509451846
	0.094191213
Average R	**0.30182153 ± 0.20763**

The above data are encouraging and allow to consider the CS-based coatings as appropriate candidates with enhanced antibacterial properties for use in food packaging applications. Further studies are underway to investigate in more detail the antimicrobial properties of these coating in real food applications.

Chapter 4: Conclusions and Future work

In conclusion, in this work water-soluble natural polymer derivatives based on chitosan were employed to coat flexible food packaging films, involving a polyethylene (PE) surface, and confer them contact-active, antibacterial properties.[4]

Before the coating process, the inert and hydrophobic polyethylene (PE) surface was treated with oxygen plasma to acquire oxygen related functional groups such as carboxyl groups and improve its water wettability. The success of the plasma treatment process was verified with static water contact angle measurements and field emission scanning electron microscopy (FESEM). The coatings, with thickness in the micrometer range, were prepared using Mayer rods, whereas their stability and adhesion onto the substrate was achieved using a cross-linker to chemically link the polymer chains among them and onto the substrate. FTIR spectroscopy and FESEM verified that both coatings were stable and remained intact onto the PE films after one month immersion in water.

The coated films presented enhanced antibacterial activity against a range of food-related bacteria, including *S. aureus*, *E. coli* and *L. monocytogenes*. Furthermore, the coatings increased the oxygen and water vapor barrier properties of the polyethylene films, without affecting their mechanical strength. The results presented in this study suggest that the developed coatings are promising for use in active food packaging technologies.

As a future work, it would be interesting to prepare modified chitosan at large scale, that would be able to reproduce the stability, thermal, mechanical, barrier and antimicrobial properties of the coatings that were presented in this study, for applications in the food industry. It would be also worth studying the antimicrobial action of the coatings when in contact with bacteria infected food.

References

1. Harrison, L. M.; Balan, K. V.; Babu, U. S., Dietary fatty acids and immune response to food-borne bacterial infections. *Nutrients* **2013,** *5* (5), 1801-1822.
2. Amri, F.; Husseinsyah, S.; Hussin, K., Mechanical, morphological and thermal properties of chitosan filled polypropylene composites: The effect of binary modifying agents. *Composites Part A: Applied Science and Manufacturing* **2013,** *46*, 89-95.
3. Manouras, T.; Koufakis, E.; Vasilaki, E.; Peraki, I.; Vamvakaki, M., Antimicrobial hybrid coatings combining enhanced biocidal activity under visible-light irradiation with stimuli-renewable properties. *ACS Applied Materials & Interfaces* **2021,** *13* (15), 17183-17195.
4. Emanuel, N.; Harloveleen, K., Food Packaging Development: Recent Perspective. *J. Thin Film. Coat. Sci. Technol. Appl* **2019,** *6*, 13-29.
5. Fotie, G.; Limbo, S.; Piergiovanni, L., Manufacturing of food packaging based on nanocellulose: Current advances and challenges. *Nanomaterials* **2020,** *10* (9), 1726.
6. Mathlouthi, M., *Food packaging and preservation*. Springer Science & Business Media: 1994.
7. Ebnesajjad, S., *Plastic films in food packaging: materials, technology and applications*. William Andrew: 2012.
8. Marsh, K.; Bugusu, B., Food packaging—roles, materials, and environmental issues. *Journal of food science* **2007,** *72* (3), R39-R55.
9. Girling, P., Packaging of food in glass containers. *Food packaging technology. London, UK: Blackwell Publishing, CRC Press. p* **2003**, 152-73.
10. Deshwal, G. K.; Panjagari, N. R., Review on metal packaging: Materials, forms, food applications, safety and recyclability. *Journal of food science and technology* **2020,** *57* (7), 2377-2392.
11. Stille, J. K., Step-growth polymerization. ACS Publications: 1981.
12. Bonillo, B.; Swager, T. M., Chain-growth polymerization of 2-chlorothiophenes promoted by Lewis acids. *Journal of the American Chemical Society* **2012,** *134* (46), 18916-18919.
13. Vasile, C., *Handbook of polyolefins*. CRC press: 2000.
14. Del Nobile, M. A.; Buonocore, G.; Palmieri, L.; Aldi, A.; Acierno, D., Moisture transport properties of polyamides copolymers intended for food packaging applications. *Journal of food engineering* **2002,** *53* (3), 287-293.
15. Bhunia, K.; Sablani, S. S.; Tang, J.; Rasco, B., Migration of chemical compounds from packaging polymers during microwave, conventional heat treatment, and storage. *comprehensive Reviews in food Science and food Safety* **2013,** *12* (5), 523-545.
16. Nisticò, R., Polyethylene terephthalate (PET) in the packaging industry. *Polymer Testing* **2020,** *90*, 106707.
17. Roberts, T., Human illness costs of foodborne bacteria. *American Journal of Agricultural Economics* **1989,** *71* (2), 468-474.
18. Anthony, B. F.; Hill, H. R., Gram-positive bacteria: an overview and summary of session. *Reviews of Infectious Diseases* **1988**, S345-S350.
19. Neu, H. C., Infections due to gram-negative bacteria: an overview. *Reviews of Infectious Diseases* **1985,** *7* (Supplement_4), S778-S782.
20. Khaneghah, A. M.; Hashemi, S. M. B.; Limbo, S., Antimicrobial agents and packaging systems in antimicrobial active food packaging: An overview of approaches and interactions. *Food and Bioproducts Processing* **2018,** *111*, 1-19.
21. Wei, T.; Zhan, W.; Cao, L.; Hu, C.; Qu, Y.; Yu, Q.; Chen, H., Multifunctional and regenerable antibacterial surfaces fabricated by a universal strategy. *ACS applied materials & interfaces* **2016,** *8* (44), 30048-30057.

22. Riga, E. K.; Vöhringer, M.; Widyaya, V. T.; Lienkamp, K., Polymer-Based Surfaces Designed to Reduce Biofilm Formation: From Antimicrobial Polymers to Strategies for Long-Term Applications. *Macromolecular rapid communications* **2017,** *38* (20), 1700216.
23. Hasan, J.; Crawford, R. J.; Ivanova, E. P., Antibacterial surfaces: the quest for a new generation of biomaterials. *Trends in biotechnology* **2013,** *31* (5), 295-304.
24. Bruenke, J.; Roschke, I.; Agarwal, S.; Riemann, T.; Greiner, A., Quantitative comparison of the antimicrobial efficiency of leaching versus nonleaching polymer materials. *Macromolecular Bioscience* **2016,** *16* (5), 647-654.
25. Ivanova, E. P.; Hasan, J.; Webb, H. K.; Truong, V. K.; Watson, G. S.; Watson, J. A.; Baulin, V. A.; Pogodin, S.; Wang, J. Y.; Tobin, M. J., Natural bactericidal surfaces: mechanical rupture of Pseudomonas aeruginosa cells by cicada wings. *Small* **2012,** *8* (16), 2489-2494.
26. Kittur, F. S.; Kumar, K. R.; Tharanathan, R. N., Functional packaging properties of chitosan films. *Zeitschrift für Lebensmitteluntersuchung und-Forschung A* **1998,** *206* (1), 44-47.
27. Qin, C.; Li, H.; Xiao, Q.; Liu, Y.; Zhu, J.; Du, Y., Water-solubility of chitosan and its antimicrobial activity. *Carbohydrate polymers* **2006,** *63* (3), 367-374.
28. Sudarshan, N. R.; Hoover, D. G.; Knorr, D., Antibacterial action of chitosan. *Food biotechnology* **1992,** *6* (3), 257-272.
29. Darmadji, P.; Izumimoto, M., Effect of chitosan in meat preservation. *Meat science* **1994,** *38* (2), 243-254.
30. Bhale, S.; No, H.; Prinyawiwatkul, W.; Farr, A.; Nadarajah, K.; Meyers, S., Chitosan coating improves shelf life of eggs. *Journal of food science* **2003,** *68* (7), 2378-2383.
31. Duan, C.; Meng, X.; Meng, J.; Khan, M. I. H.; Dai, L.; Khan, A.; An, X.; Zhang, J.; Huq, T.; Ni, Y., Chitosan as a preservative for fruits and vegetables: a review on chemistry and antimicrobial properties. *Journal of Bioresources and Bioproducts* **2019,** *4* (1), 11-21.
32. Tayel, A. A.; Moussa, S.; Opwis, K.; Knittel, D.; Schollmeyer, E.; Nickisch-Hartfiel, A., Inhibition of microbial pathogens by fungal chitosan. *International journal of biological macromolecules* **2010,** *47* (1), 10-14.
33. Ellison, A.; Zisman, W., Wettability studies on nylon, polyethylene terephthalate and polystyrene. *The Journal of Physical Chemistry* **1954,** *58* (6), 503-506.
34. Lehocký, M.; Drnovská, H.; Lapčíková, B.; Barros-Timmons, A.; Trindade, T.; Zembala, M.; Lapčík Jr, L. r., Plasma surface modification of polyethylene. *Colloids and Surfaces A: Physicochemical and Engineering Aspects* **2003,** *222* (1-3), 125-131.
35. Amelinckx, S.; Van Dyck, D.; Van Landuyt, J.; van Tendeloo, G., *Electron microscopy: principles and fundamentals*. John Wiley & Sons: 2008.
36. Igarashi, S.; Mita, I.; Kambe, H., Thermogravimetric analysis of polyoxymethylene. *Bulletin of the Chemical Society of Japan* **1964,** *37* (8), 1160-1165.
37. Mutsaers, M., Near infrared spectroscopy as a diagnostic tool in surveillance of arboviral vector control, predicting Wolbachia infection in post-mortem Aedes aegypti. **2018**.
38. McMurry, J. E., Organic Chemistry. **2012**.
39. https://mechanicalc.com/reference/mechanical-properties-of-materials.
40. Johansson, F.; Leufvén, A., Influence of sorbed vegetable oil and relative humidity on the oxygen transmission rate through various polymer packaging films. *Packaging Technology and Science* **1994,** *7* (6), 275-281.
41. Sprockel, O.; Prapaitrakul, W.; Shivanand, P., Permeability of cellulose polymers: water vapour transmission rates. *Journal of pharmacy and pharmacology* **1990,** *42* (3), 152-157.
42. Yuan, Y.; Lee, T. R., Contact angle and wetting properties. In *Surface science techniques*, Springer: 2013; pp 3-34.

43. Gill, P.; Moghadam, T. T.; Ranjbar, B., Differential scanning calorimetry techniques: applications in biology and nanoscience. *Journal of biomolecular techniques: JBT* **2010,** *21* (4), 167.
44. Cashera, A.; Porosa, L., ISO 22196: 2011 Measurement of antibacterial activity on plastics and other non-porous surfaces "Modified Large droplet Inoculation Method.".
45. Lavertu, M.; Xia, Z.; Serreqi, A.; Berrada, M.; Rodrigues, A.; Wang, D.; Buschmann, M.; Gupta, A., A validated 1H NMR method for the determination of the degree of deacetylation of chitosan. *Journal of pharmaceutical and biomedical analysis* **2003,** *32* (6), 1149-1158.
46. Zou, X.; Zhao, X.; Ye, L., Synthesis of cationic chitosan hydrogel with long chain alkyl and its controlled glucose-responsive drug delivery behavior. *RSC advances* **2015,** *5* (116), 96230-96241.
47. Wang, W.-P.; Du, Y.-M.; Wang, X.-Y., Physical properties of fungal chitosan. *World Journal of Microbiology and Biotechnology* **2008,** *24* (11), 2717-2720.
48. Cava, D.; Catala, R.; Gavara, R.; Lagaron, J. M., Testing limonene diffusion through food contact polyethylene by FT-IR spectroscopy: film thickness, permeant concentration and outer medium effects. *Polymer Testing* **2005,** *24* (4), 483-489.
49. Colomer, M., Straightforward synthesis of Ti-doped YSZ gels by chemical modification of the precursors alkoxides. *Journal of sol-gel science and technology* **2013,** *67* (1), 135-144.
50. Zhang, M.; Lynch, D. T.; Wanke, S. E., Characterization of commercial linear low-density polyethylene by TREF-DSC and TREF-SEC cross-fractionation. *Journal of applied polymer science* **2000,** *75* (7), 960-967.
51. Burfield, D. R.; Kashiwa, N., DSC studies of linear low density polyethylene. Insights into the disrupting effect of different comonomers and the minimum fold chain length of the polyethylene lamallae. *Die Makromolekulare Chemie: Macromolecular Chemistry and Physics* **1985,** *186* (12), 2657-2662.
52. Millot, C.; Fillot, L.-A.; Lame, O.; Sotta, P.; Seguela, R., Assessment of polyamide-6 crystallinity by DSC. *Journal of Thermal Analysis and Calorimetry* **2015,** *122* (1), 307-314.